Results of Molecular Dynamics Calculations

Herbert M. Urbassek

Fachbereich Physik, Universität Kaiserslautern,
Erwin-Schrödinger-Straße, 67663 Kaiserslautern, Germany
urbassek@rhrk.uni-kl.de

Abstract. In recent years, the method of molecular-dynamics computer simulation has increasingly been employed to investigate the mechanisms underlying sputtering of solids by ion and cluster impact. This review highlights the results obtained by this method. The topics covered include sputtering in the linear-cascade and the spike regime, cluster emission, the formation of surface topography by sputtering and its effects on sputtering, sputtering of molecular solids and chemical effects in sputtering.

1 Introduction

Sputtering [1–4] is the process of emission of (neutral or charged) atoms due to the bombardment of the surface of a material by energetic particles. Usually these projectiles are ions, but as well atoms, clusters or other particles (neutrons, electrons, etc.) may be employed.

The theoretical understanding of the sputter phenomenon is quite advanced. While the main progress in the theoretical description of the sputter phenomenon came by analytical theory [5], computer simulations were increasingly used throughout the last decades to investigate ion irradiation-induced phenomena. Simulation algorithms based on the so-called 'binary collision approximation' (BCA) as well as various Monte Carlo schemes were set up to study processes in structureless [6] and crystalline [7] targets; they are reviewed in [8] and elsewhere in this book.

Molecular dynamics simulations have been employed for a long time to obtain an atomistic understanding of irradiation-induced processes. Indeed one of the earliest applications of the method has been a seminal contribution by *Vineyard* et al. [9], who applied molecular dynamics to the study of primary knock-on processes in metals. This was only three years after this method was invented to study the equilibrium properties of a hard-sphere fluid [10].

There are good reasons to apply molecular dynamics to sputtering:

1. A complete description of the projectile-surface interaction process starts with the projectile slowing down in the target and ends with the dissipation and finally thermalization of the energy. The molecular dynamics

R. Behrisch, W. Eckstein (Eds.): Sputtering by Particle Bombardment,
Topics Appl. Physics **110**, 189–230 (2007)

method is, in principle, able to follow this whole sequence of events without any further assumptions or approximations, once the interatomic interaction potentials and the electronic stopping have been specified.
2. Material dependent parameters – like surface binding energies, nuclear stopping powers, melting or boiling temperatures – are included naturally in the interatomic interaction potentials. Thus with a realistic specification of these potentials, no further ad hoc parameters need to be introduced.
3. The effects of bonding and reactions, which are particularly important for the sputtering of molecules and clusters, but also for the sputtering of non-elemental and in particular molecular solids, are included in a straightforward way, once the appropriate potentials have been formulated.
4. The effects of a nanoscopic structure of the surface – atomic roughness or surface topography – are easily included in the simulation.

A draw-back of the method of molecular dynamics is that it is able to study the processes only for a short period of time (roughly < 1 ns) and on small spatial scales (in target volumes comprising some millions of atoms, say). While these limits may change with the development of hard- and software, it is a difficult task to stretch the simulation to the time and space scales over which real experiments extend. The methods of analytical sputter theory (transport theory), and the binary-collision-approximation Monte-Carlo methods easily transgress these restrictions in time and space scales.

An advantage of the method is that it lends itself easily to the visualisation of the processes occurring and even to their animation. Thus the graphical presentation of the data obtained is often appealing to imagination and may provide for a deeper understanding of the processes occurring.

Since the early days of the application of molecular dynamics to ion-irradiation and sputtering processes, a number of reviews have appeared [8, 11–16]. These cover both the methods applied and the simulation results obtained. The aim of the present review is to delineate the lines of development of the method to show 1. where molecular dynamics has been used intensely in sputter physics; 2. where molecular dynamics has contributed to an understanding of sputter physics. While no complete coverage of the literature is possible, it is hoped that the main lines of development can be shown here.

The progress in this method is established both in the development of hardware and software. Trivially, progress in hardware capacities allows for the simulation of larger targets – this allows for an increase of the bombarding energy which can realistically be studied – and the simulation of a larger number of impact events, which increases the significance of the data obtained. The development in software leads to:

1. The formulation of better potentials, which describe the materials behaviour; these are in particular important for the description of chemical effects and the bombardment of molecular solids.

2. The formulation of better boundary conditions of the simulation crystallite which allow to better control the effects of the finite size of the simulation target in contrast to the experiment.
3. The inclusion of further effects in the molecular dynamics simulation, such as electronic effects in sputtering (excitation or ionization).

In this contribution, the impact of molecular dynamics simulations on the understanding of the physics underlying the sputter phenomenon is presented and discussed. While a complete coverage of all scientific contributions to this subject appears impossible, it has been attempted to sketch the various fields in which molecular dynamics simulations have proven fruitful to widen and deepen our understanding. Due to the atomistic nature of this simulation technique, as diverse aspects as cluster impact, chemical effects in sputtering, or the effect of surface topography on sputtering could benefit from this method.

2 Linear-Cascade Regime

A number of molecular dynamics studies have been performed in order to investigate basic issues in linear sputtering theory. The grouping of the results reported below under this heading may not appear fair in all cases. However, this section is meant to contain all those results that can be understood at least in a first approximation from the assumptions underlying linear-cascade theory, and refer to processes where neither atomic binding nor high energy densities play a strong role.

Single-crystalline targets are implemented with particular ease in molecular dynamics; hence several studies on clarifying the sputter mechanisms of single crystals have been performed. The evolution of this field until 1992 is described in [17]. A special impetus for performing these simulations is provided by experimental techniques which allow to measure energy-resolved angular distributions of sputtered particles for small irradiation fluences and hence under well defined surface conditions. Such an experimental situation lends itself in an ideal way to molecular dynamics simulations. In fact, it may be hoped that here it is only the interatomic interaction potential the knowledge of which limits the accuracy of the simulation. In this situation, a new potential – due to *DePristo* et al. [18, 19] – was incorporated into the simulation, which was believed to describe interatomic interaction in metals in a more accurate way, and the sputter calculations which were previously performed with the established embedded-atom-method (EAM) potential [20] were repeated. The new results appear to show a better agreement with experimental data [21].

Among further work on single-crystal sputtering we wish to mention [22], which aimed at identifying the mechanism of Wehner spot formation for low-energy sputtering, i.e., the preferential emission of sputtered atoms in

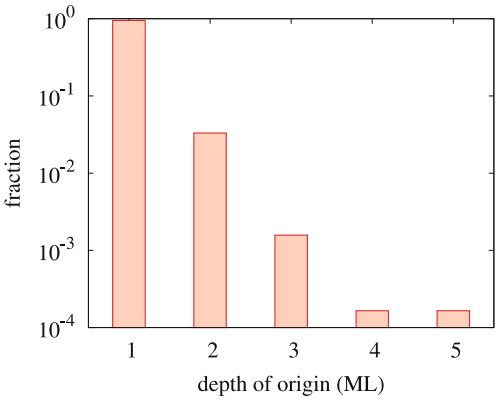

Fig. 1. Distribution of depth of origin of Cu atoms sputtered by 1 keV Ar ions from a Cu (100) surface. Molecular dynamics data from [30]

close-packed crystal directions. Also [23] and [24] investigated this subject with a particular interest in the temperature dependence of Wehner spots. Sputtering induced by hyperthermal rare-gas atoms bombarding different low-indexed surfaces of a Cu crystal was investigated in [25]. Other work tried to identify the differences between the sputtering of an amorphous in contrast to a single-crystal Si surface [26]; there also several discrepancies with previous simulation results of crystalline Si sputtering [27, 28] are discussed. The depth of origin of sputtered atoms was studied using molecular dynamics (and Monte Carlo) simulations in [29] for random target orientation. Figure 1 exemplifies the distribution of depth of origin for 1 keV Ar impact on a Cu (100) surface. It shows that some 95 % of the sputtered atoms originate from the topmost surface layer for impact on a (100) surface; on a (111) surface it is only 85 % [23].

Finally, some unusual work on linear-cascade sputtering should be mentioned. In condensed gases, very low-energy atoms – in the eV region – may give rise to so-called mini-cascades [31]. Such low energy atoms may be excited for instance by electronic excitation, and subsequent energy transfer to atomic motion. Molecular dynamics simulations of this phenomenon have been performed with the aim of describing electronic sputtering in condensed gases [32] and the transmission of atoms through thin rare-gas films, and the concomitant sputtering [33].

In summary, the method of molecular dynamics is well able to study sputtering in the linear-cascade regime. Since, however, the BCA method is readily applied to this regime, and with less expenses in computer time, molecular dynamics simulations are in general only performed in those cases where either the binding situation in the target needs to be accurately implemented (such as in compounds), the number of approximations introduced needs to be minimized in order to study a small effect (such as in prefer-

ential sputtering of isotopes) or simply advantage is drawn from the ready availability of the molecular dynamics program. Two specific areas where molecular dynamics simulations have been successfully used in this respect are discussed in the following.

2.1 Low-Energy Sputtering

The sputtering behaviour for low-energy impacts ($< 1000\,\text{eV}$, say) lends itself readily to molecular-dynamics simulation. *Kress* et al. [34] investigate the low-energy off-normal Ar and copper bombardment of Cu (111). *Gades* and *Urbassek* [25] investigate energy deposition, reflection and sputtering of normal-incidence rare-gas atoms with energies of 5–400 eV off polycrystalline Cu, and compare to experimental measurements by *Winters* et al. [35, 36]. Good agreement is obtained for the energy dependence of the deposited energy. Light projectiles deposit less energy in the target due to their increased reflection probability; for heavy projectiles, sputtering is the dominant energy loss channel from the target. *Abrams* and *Graves* [37, 38] study sputtering of Cu by Ar and Cu low-energy impacts ($< 175\,\text{eV}$). They discuss the sputtering and the sticking coefficient as a function of the incidence angle and state favourable agreement of their sputtering yields with the experimental data compiled in [39]. The same authors also study sputtering of rough SiO_2 surfaces by obliquely incident low-energy Ar atoms [40] and emphasize the angular and energy distributions of sputtered atoms and molecules. *Kubota* and *Economou* [41] investigate the growth of a thin oxide film on Si induced by thermal O atoms and sputtering by 100 eV Ar ions.

Several low-indexed surfaces of fcc and bcc crystal have been reinvestigated by *Shapiro* et al. [42]. *Güvenc* et al. [43] discuss the sputtering mechanism, including the effect of the projectile-target interaction potential, on the sputtering yield of the Ar $\rightarrow$ Ni (100) system for bombarding energies between 10 and 40 eV. They find the theoretical yields to be considerably higher than the experimental yields [44] and attribute this discrepancy to the incomplete knowlegde of the real interatomic potential functions.

2.2 Preferential Sputtering

The sputtering behaviour of compounds and alloys is of considerable practical interest [45]. In these materials, sputtering yields, but also the angular and energy distributions, will depend on the species that is ejected. In other words, the measurement of *partial* yields and distributions is of prime interest.

Let us concentrate in the following on the sputtering of a binary system of species i and j which are homogeneously mixed with concentrations c_i, c_j, where $c_i + c_j = 1$. While after irradiation with sufficiently high fluence, a steady state will be reached, in which the ratio of the sputtering yields is stoichiometric, i.e., equals the ratio of the bulk concentrations,

$$Y_i/Y_j = c_i/c_j\,, \tag{1}$$

this is in general not the case for small fluences. We shall call the normalized ratio

$$\delta = \frac{Y_i}{Y_j}\frac{c_j}{c_i} \tag{2}$$

the sputter preferentiality, since its deviation from the value 1 indicates over- or under-stoichiometric emission of a particular species. Note that in some papers, $(\delta - 1)$ is called the sputter preferentiality. Analytical sputter theory [46] predicts δ to depend on the masses $M_{i,j}$ and the surface binding energies $U_{i,j}$ of the respective species in the alloy as

$$\delta = \left(\frac{M_j}{M_i}\right)^{2m} \left(\frac{U_j}{U_i}\right)^{1-2m} . \tag{3}$$

Here m denotes the power exponent describing the interaction potential.

The sputtering of such a system is of considerable interest to SIMS. The static SIMS case corresponds to low fluences, $\Phi \to 0$, while the interpretation of dynamic SIMS data needs (among others) a knowledge of the dependence of the partial sputtering yields on fluence Φ. A wealth of experimental data as well as (dynamic) binary-collision simulations is reviewed in *Gnaser* [47], and elsewhere in this volume.

Molecular dynamics simulations on sputtering of multi-component materials are comparatively rare. In the following, only results on the static case ($\Phi \to 0$) will be reviewed. *Gades* and *Urbassek* [48] studied the preferential sputtering of a series of model alloys CuX. By choosing X as a pseudo-copper species which is more weakly (strongly) bound than natural copper, the dependence of the preferential sputtering on the surface binding could be explored. Here it was shown that – in particular for low bombarding energies of 1 keV – the simulated preferentiality is stronger than in the analytical estimates; with increasing bombarding energy the analytical estimate appears to describe the simulation data better.

A special case of particular interest is the sputtering of isotopic mixtures. Here sputtering is governed by the mass ratios of the different isotopes in the specimen. Equation (3) thus predicts a preferentiality

$$\delta = \left(\frac{M_j}{M_i}\right)^{2m} . \tag{4}$$

Since this effect is generally small, in the percentage range, in molecular dynamics simulations the mass differences are often artificially enhanced in order to increase the preferentiality, and hence improve the statistical significance of the results [49]. Early work was performed by *Shapiro* et al. [50, 51] who considered a variety of targets (both two- and three-isotope crystals and liquids) and compositions. The preferentiality showed a size compatible with the experimental findings. Large emission-angle-dependent effects were

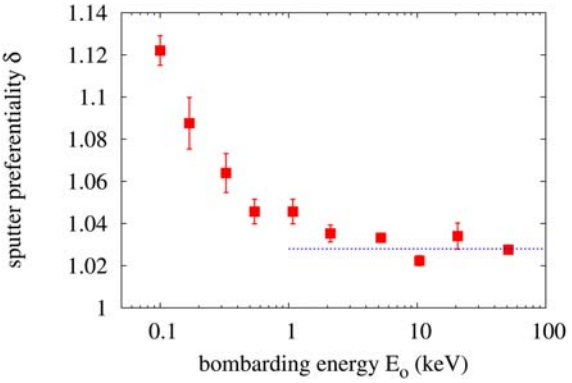

Fig. 2. Computer simulation data [54] for the sputter preferentiality δ in a 1:1 stoichiometric mixture of ^{92}Mo and ^{100}Mo, sputtered by Ar ions of energy E_0. δ shows a strong dependence on the ion impact energy; only for sufficiently high energy, $E_0 > 10\,\text{keV}$, the asymptotic result, (4), with $m = 1/6$ (*dotted line*) is retrieved

found, and a strong dependence on the target crystallinity, such that liquid samples, deviated strongly in their angular emission pattern from crystalline samples.

In their study of model CuX alloys, *Gades* and *Urbassek* [48] also chose X as a heavy copper atom with twice the natural mass. A sputter preferentiality of $\delta = 1.30 \pm 0.05$ was obtained, in good agreement with the theoretical value 2^{2m}, where $m = 0.19$ for the potential adopted.

Lam and *Johannessen* [52] studied the preferential sputtering of CuNi; this study was later repeated by *Gades* and *Urbassek* [48]. The resulting preferentialities of $\delta = 1.22$ and 1.25, respectively, of the two simulation studies coincide; in this case the preferentiality originates mainly from the different surface binding energies of copper and nickel in the specimen.

Shulga and *Sigmund* performed a series of simulations, where besides binary-collision simulations also molecular dynamics was employed [53, 54]. Molybdenum isotope samples with an artificially increased mass ratio were investigated. These authors studied in particular the dependence of the preferentiality on the bombarding ion energy, and showed that the theoretical result is only retrieved for high energies ($E_0 > 10\,\text{keV}$ in their case), cf. Fig. 2. At low bombarding energies, the sputter preferentiality strongly depends on the mass and energy of the bombarding species and varies considerably with the emission angle; this effect could be reduced to the collision kinematics of binary scattering.

3 Ionic Crystals

Sputtering of ionic crystals has been investigated experimentally; it is known to give rise to considerably larger sputtering yields than those expected from collisional theory [55]. This is believed to be due to 'electronic sputtering', i.e., long-lived electronic excitation states which are created by the bombardment, diffuse to the surface and induce sputtering there. This process has been studied in alkali halides with quite some detail [56].

Ionic bonding occurs in many materials of practical interest. Thus, e.g., alkali halides are used for radioactive waste storage. Other relevant materials, such as SiO_2, but also SiC, and many non-metallic compounds, exhibit at least partial ionic bonding. In molecular solids, the molecular constituents may be polar, possessing permanent dipole moments; the outstanding example is given here by water. In all these cases, the long-range nature of the Coulomb (or dipole) forces complicates the strict calculation of the attractive forces used for molecular dynamics. Usually, the Coulomb contribution to the forces is ignored or cut off, when calculating the effect of ion irradiation on these compounds. Thus, e.g., in a molecular dynamics simulation of Coulomb explosion from a fast-ion-induced ion track [57], the Coulomb forces enter the simulation with an exponential screening factor $\exp(-r/a)$ and are furthermore cut off at $r_c = 7a$. In a related case, the laser ablation of water, the dipole force is cut off at a relatively short distance [58].

Nordlund [59] studies radiation effects induced by keV Ga PKA's in the strongly ionic compound GaN. By comparing the simulation results of a non-ionic model to those of an ionic charge-transfer model, he can demonstrate that in this case, the inclusion of explicit ionicity shows no strong effect on collision cascade development. In agreement with experiments [60, 61], he finds an amorphisation dose which is considerably higher in this material than in Si or comparable semiconductors; based on his simulations he attributes this effect to a high threshold displacement energy and cascade-induced annealing of damage as well as to in-cascade annealing.

Only few investigations have been published in which the long-range electrostatic forces have been fully taken into account. A recent paper by *Ramasawmi* et al. [62] investigates the sputtering of NaCl by 1 keV Na impact. Technically, these authors consider the target as a free crystallite, with fixed lateral boundaries. In this way, all electrostatic forces are taken into account for the 2 ps during which the simulation is performed. The results show a relatively low sputtering yield of 0.36 attributed to a large amount of channeling. A large number of dimers, often neutral, are emitted. Recent studies by *Young* [63, 64] model the Coulomb explosion spike in KCl and LiF crystals containing 12,800 particles generated by a swift ion. While sputter processes are not considered here, this work gives insight into the dynamical effects associated with ion track formation in such a material, affecting in this case a cylindric region of 78 Å in diameter.

4 Effect of Electronic Energy Loss and Electronic Excitations in Atomic Collision Cascades

Another thread of work attempts to identify the role of electronic inelastic loss processes in a cascade, and of electron excitation [65–67]. Such a procedure requires an *ad hoc* introduction of electronic processes into the simulation. The results achieved were also used to assess the mechanisms by which core-excited atoms are sputtered [68].

Besides giving away their energy in elastic collisions with other atoms, atoms may be slowed down in the solid also by the so called electronic stopping, i.e., inelastic losses with target atoms or the 'friction' in the electron gas of the target. This electronic stopping can be described as a velocity-proportional friction; the proportionality coefficient has been calculated by *Lindhard* and *Scharff* [69] and *Firsov* [70] and also in later more recent work [71, 72]. Such a stopping process can be included as a friction force in molecular dynamics simulation. This friction dampens the motion of the projectile but also of each target atom in the collision cascade of the solid [73].

As a consequence, projectile ranges are shortened, but also the lifetime of thermal spikes is reduced [74–76]. Since for low atom velocities, the electronic stopping has to obey the same physics as, e.g., electron-atom scattering in electrical conduction, the low-energy stopping can alternatively be described by the electron-phonon interaction [77, 78]. The magnitude of the proportionality coefficient entering the velocity-proportional stopping at low velocities has been subject to considerable debate in the past [78]. Note that recent experiments [79] allow to measure directly the kinetic electron excitation in atomic collision cascades.

Several schemes have been employed to include electronic excitation processes into the molecular dynamic simulation of collision cascades.

1. Electron promotion in close binary encounters may form the basis of excitation [80–82]. This treatment has also been applied to describing the sputter emission of highly excited metastable atoms [83, 84].
2. Low-energy atom motion (below 1 eV, say) has been modelled to couple via the electron-phonon interaction to electrons. This approach has been used to describe effects like defect production and ion-beam mixing [85]; we note that the importance of including electron-phonon coupling for these phenomena is still under discussion [76]. Assuming thermalization of the electronic and the atomic systems separately, this regime can be described by a two-temperature model [86, 87].
3. At energies above 1 eV/atom, the coupling of atomic motion to the electronic subsystems may be described by the electronic stopping power of individual atoms [88].

4.1 Stopping

The consequences of the electronic stopping of the projectile on the sputtering process are considered small and are mostly connected to the reduction of the deposited nuclear energy density; as a consequence the sputtering yield may be somewhat reduced [89].

4.2 Excitation

An interesting consequence of the energy loss into the electronic system is that it may serve as input to models of atom excitation or ionisation; these processes are of immediate interest to sputtering of ions and hence to SIMS experiments. While this idea has been exploited by *Sroubek* in several papers in the past [90, 91], recently this model was also incorporated in molecular dynamics simulations of atomic collision cascades [92]. Since the parameters describing the electronic excitation – besides the proportionality constant of the velocity-proportional friction, also the electronic mean-free path enters the problem. which is itself dependent in particular on the structure (melting, amorphisation) of the irradiated crystal [85] – are not all precisely known, such simulations have at the time being model character and allow the prediction of qualitative features rather than of quantitative effects. Nevertheless, the simulation showed that transient electronic temperatures reaching several thousand Kelvin may be reached in the vicinity of the surface and can thus influence the ionization properties of sputtered atoms.

5 High-Energy-Density (Spike) Phenomena

As soon as the energy imparted per atom E_{atom} in a certain subvolume of the cascade becomes of the order of the cohesive energy E_{coh} of the solid, or above, the linear-cascade sputter regime is left, and a so-called high-energy-density zone, or a (thermal or elastic-collision) spike is created. If this high-energy-density zone is established close to the surface, intense sputtering may result. We note that the idea that regions of high energy density are relevant for sputtering is rather old [46].

Early research concentrated on the investigation of spikes in metals. Thus for example it was established experimentally that at energies around the maximum of the nuclear stopping power, spikes contribute substantially to the sputtering of Au by heavy projectiles [93, 94]. The molecular dynamics simulation study of *Ghaly* and *Averback* [95] could visualise the spike induced by 20 keV Au bombardment of a Au target; for the trajectory shown dramatic atom emission resulted (cf. also Fig. 3).

Clear evidence of spikes was presented in simulations of keV atom bombardment of condensed rare gases [96, 97]. More recently, also the transition from collision-cascade to spike (or from linear to nonlinear) sputtering was

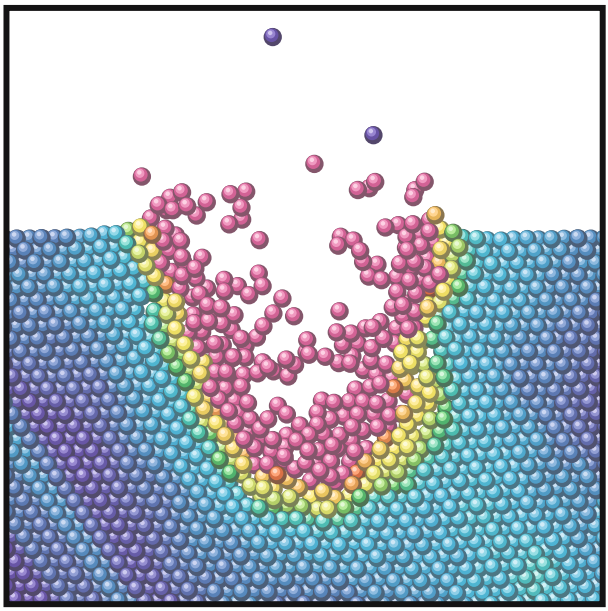

Fig. 3. Cross section through a Au crystal 1.5 ps after perpendicular impact of a Au_{13} cluster with 10 keV total energy on its (111) surface. Color denotes local 'temperature'; the *green zone* corresponds to the melting temperature, the *red zone* has reached double this temperature

investigated in such systems [98]. In the (nonlinear) spike regime, the molecular dynamics analysis of such events allowed to describe the phenomena occurring after atom impact using hydrodynamical and thermodynamical quantities:

1. a low particle density in the spike region, which has been created due to the high pressure established there;
2. an explosion-like velocity distribution leading to a radial expansion of the material around the 'centre of the spike'; this velocity distribution leads to the correlated outward emission of the surface of the energized cascade volume;
3. a huge sputtering yield, resulting in the formation of a crater;
4. the energy distribution of emitted atoms exhibits a $1/E^2$-tail for higher energies ($E > 0.2$ eV in the case of an Ar target) in agreement with linear-cascade theory. Below 0.1 eV an excess amount of low-energy particles are sputtered; these particles are associated with the thermal-spike character of the emission.

The last two features have been observed experimentally [99–101]. Spikes may be rather long lived – on the order of 1 to several ps –, whereas linear collision cascades have died several 100 fs after ion impact, when the energy of all

atoms has decreased below the cohesive energy, and hence no more collision-cascade sputtering can occur. The reason hereto is that in a spike, energy has more or less been equilibrated between all the atoms, and hence its lifetime is governed by energy diffusion (heat conduction) out of the spike volume, while in a linear collision cascade each moving atom loses energy when it collides with an atom at rest. Hence it is a question of major importance for the lifetime of spikes whether electrons can participate in energy dissipation. Various schemes have been proposed to include electrons into a molecular dynamics simulation in a phenomenological way [14, 73, 77, 85, 86, 88]. One result of these considerations is that for good electrical conductors – such as Cu or Ag – the coupling between electrons and atoms is too small to sensibly affect the lifetime of a spike; in other cases, however, – such as Ni or Pt – spikes may be efficiently quenched by electronic heat conduction [77, 86]. Even arguments were raised that in some cases energy may be imparted from the electrons to the phonon systems. Such a situation may be important for high-energy irradiation (in the MeV region) where a nonnegligible part of the projectile energy is given to the electronic system, and may be imparted from the electrons to the atoms [87].

In the following Sect. 5.1, results on sputtering from fast-ion-induced tracks will be presented, since these offer a situation in which high energy densities are imparted to the target. High energy densities also occur for cluster impact; the sputtering induced in this situation will be reviewed in Sect. 5.2. In cases where a spike has been formed due to ion or cluster impact, a crater may be produced at the surface, see Sect. 7.2. Finally, Sect. 10.2 reviews simulation results on the sputtering of molecular and organic solids, in which often – due to the low cohesive energy of the materials – a situation of a high-energy-density zone will be produced.

5.1 Sputtering from Fast-Ion-Induced Tracks

Sputter emission from fast-ion-induced tracks in the electronic-stopping regime, i.e., at energies, where the electronic stopping dominates the nuclear stopping, was analysed using molecular dynamics in the last decade. These tracks are produced by swift ions, typically fission fragments, which penetrate on a straight line deep into the material and deliver energy mainly in the form of electronic excitation. Close to the surface, the high energy deposition may induce sputtering from these tracks. Molecular dynamics simulations usually skip the details of how the electronic energy is converted into nuclear motion and immediately assume the excitation energy to be imparted as random kinetic energy of the atoms.

Often a model system has been chosen for simulation; it consists of a van-der-Waals bonded material, described by a Lennard-Jones potential. The initial excitation in the fast ion track is modelled as a cylindrical region extending into the target which is filled with excitation energy. The processes

occurring in the material after this initial energization are followed using molecular dynamics.

An early paper by *Fenyö* et al. [102, 103] showed that molecular dynamics simulation is able to analyze this process. Later *Kafemann* et al. [104] discussed the dependence of the sputtering yield on the radius of the cylindrical excitation region and on the energy density in this region. They showed the existence of two sputter regimes: A threshold or onset regime, in which the sputtering yield depends highly nonlinearly on the excitation energy density, and a higher-energy linear regime. In a series of papers, *Bringa* and *Johnson* analysed this scenario in greater detail. The following results could be obtained [105–108]: 1. A third regime was identified where at low densities of the energetic excitation events the yield is linear due to the sparse distribution of the excitations [109]. 2. The high-energy-density linear regime is connected to the formation of a melt and the removal of energy by a pressure pulse. In this regime the size of the yield increases with the initial radial extension of the track and is determined by the removal of energy radially by the pressure pulse and by the transport of energy from depth to the surface.

This analysis was later corroborated by comparison to fluid-dynamic calculations [110–113]. These ascribe the linear dependence of the yield on the excitation density by a competition of cooling of the cascade and mass ejection from the surface.

In [57] *Bringa* and *Johnson* analyse the Coulomb explosion of a cylindrical ionisation track using molecular dynamics and compare it to sputtering by a spike. They argue that Coulomb explosion and spike refer to the early and late aspects of the ionisation track produced in a solid by a fast incident ion.

Beuve et al. [114] study two further aspects of fast-ion-induced sputtering by including the dynamics of the electronic subsystem: 1. the energy transfer from the electronic to the atomic system is assumed not to occur instantaneously but to take a period of time Δt. For $\Delta t > 1\,\mathrm{ps}$ it is found that the sputtering yield becomes strongly nonlinear as a function of the stopping power. 2. The influence of a non-homogeneous spatial distribution of the electronic excitations is modelled. It is shown that such a spatial distribution also leads to a strongly non-linear dependence of the yield on the excitation density.

5.2 Cluster Impact

In recent years, the consequences of energetic cluster impact on solids have received increased attention. Thus, the consequences of bombarding surfaces with clusters have been investigated by molecular dynamics for the purpose of identifying the basic interaction mechanisms of clusters with solids [115–122], and to model cluster deposition [123–126]. Besides sputtering, the induced surface modification and defect formation [127, 128], cluster ranges [129, 130], surface growth (thin-film deposition) [123, 126] and surface smoothing [131–133] have been investigated.

Early investigations of molecular dynamics simulations of sputtering induced by cluster impact include [116, 134] and are reviewed in [94]. In terms of sputtering physics, cluster impact, in particular for large cluster sizes, represents a clear-cut example for spike sputtering. Figure 3 gives an atomistic view of the processes occurring in a crystal shortly after impact of a large cluster.

5.2.1 Small Cluster Impact ($n \leq 3$)

Lindenblatt et al. [135] performed a detailed study of Ag_n ($n = 1, 2, 3$) bombardment of the Ag (111) surface at 2 keV/atom. Besides the total sputtering yields, the cluster abundancies in the flux of sputtered particles were determined. For the case of Ag_2 and Ag_3 projectiles, a pronounced dependence of the yields on the orientation of the projectiles could be observed. The authors show that polyatomic projectiles produce colder sputtered clusters.

Medvedeva et al. [136] study similarly the sputtering of a Si (100) surface by Al_n and Au_n clusters with 1.5 keV/atom incidence energy for sizes $n = 1$ and 2. This study emphasizes the role of an oblique incidence angle in producing high sputtering yields and enhanced probability for producing clusters.

Shapiro and *Tombrello* [137–139] study the sputtering of a Au (111) surface with 100 keV/atom Au_n ions ($n = 1$, 2, 3). They restrict their attention to the first 3 ps after projectile impact and hence to the collision-cascade phase and the earliest phase of the thermal spike; angular and energy distributions of atoms sputtered during this time are discussed.

5.2.2 Larger Cluster Impact ($n > 3$)

Insepov and co-workers have published the results of a series of investigations performed over the years [127, 128, 131, 140–143]. They are interested in large cluster impacts with sizes between several 10 and 10^4 atoms. While their main interest is the modification of the target, also the results of sputtering have been published. In [140] *Insepov* and *Yamada* study Ar_n cluster impact with energies of between 10 and 100 eV/atom for sizes $n = 55-200$. They calculate the sputtering yields of a Au and a Si target and show that cluster bombardment induces sputtering of clusters more efficiently than atom bombardment. In [128] these studies are extended to applications such as surface-smoothing under cluster-beam irradiation, which is discussed in Sect. 5.2.3 below. In these studies as well as in [131] also the angular distribution of sputtered atoms is obtained which shows preferential ejection at rather oblique angles. In [142] besides sputtering yields also the scaling of the crater depth with the total cluster energy E for Ar_n impact on a Cu (100) surface is calculated and shown to obey a $E^{1/3}$ power law. In this study, the impact energies range between 6.4 and 20 keV and the cluster sizes between 236 and 736 atoms.

Betz and *Husinsky* [144] examine Al_n cluster impact on Cu (111) with energies between 0.1 and 30 eV/atom and cluster sizes between $n = 60$ and 1080.

They study the transition between cluster deposition and surface erosion, and emphasize the role of the local deposition 'temperature' on the eventual fate (melting, mixing with the surface, evaporation, ...) of the cluster.

Sputtering of the Au (111) surface induced by Au_n clusters ($n = 1 - 12$) at fixed total energy of 16 keV is discussed by *Colla* et al. [145] and *Colla* and *Urbassek* [146]. They obtain the following results:

1. Sputtering lasts a long time (> 8 ps) with the exception of monomer bombardment.
2. Pronounced craters are formed as a rule on initially flat surfaces.
3. Large clusters are emitted late from the crater rim and contribute substantially to the sputtering.
4. Sputter-yield fluctuations – originating from varying cluster orientations and impact points on the surface – decrease with increasing cluster size.

Colla and *Urbassek* [146] also study equi-velocity Au_n ($n = 1, 2, 4$) clusters at an energy $E/n = 16$ keV/atom. *Salonen* et al. [147] extend these studies to Au_n cluster impact with n up to 65600 at a total energy of 25 keV. They show that the cluster yield is more or less constant for cluster sizes $n = 2 - 7600$, giving evidence that the total energy determines the sputtering yield in this regime.

Yamaguchi and *Gspann* [148] study cluster impacts on the diamond (111) surface; both Ar_n and $(CO_2)_n$ clusters with a size of $n \cong 1000$ are used. Total impact energies between 10 and 100 keV are studied. Besides an analysis of the temporal evolution of kinetic and potential energies and the temperatures in the system, the dependence of the crater volumes on the bombarding energy is analysed. Furthermore this study shows a considerable enhancement of the sputtering by CO_2 clusters with respect to those of an Ar cluster impact and attribute it to chemical sputtering, i.e., the reactive enhancement of surface erosion by C-O chemistry.

Simulation of fullerene bombardment and the induced sputtering has early been attacked by molecular dynamics [149]. More recently, *Postawa* et al. [150] compare the consequences of a C_{60} cluster impact and a Ga atom impact, each with 15 keV (total) energy, on Ag (111). C_{60} bombardment leads to a yield enhancement by a factor 16 and the yield of Ag_3 is enhanced by a factor of 35. The reason hereto is assigned to the fact that C_{60} deposits its energy close to the surface, thus providing for an efficient means for sputtering.

Zhurkin and *Kolesnikov* [151] report on the sputtering of Al and Ni_3Al induced by Al_n equi-velocity clusters with energies of 100 and 500 eV/atom and sizes between $n = 1$ and 55. The authors discuss the dependence of the sputtering yield on the cluster size, and also give data on the preferential particle ejection from the compound target.

5.2.3 Cluster-Induced Surface Smoothing

Sputtering by cluster bombardment has been used to reduce the atomistic roughness of surfaces. This process, which has been termed 'ion-beam polishing'or 'ion-beam milling' when performed with obliquely incident ions bombarding a rotating target surface, has been found to proceed efficiently when using clusters to smoothen the surface [131].

Moseler et al. [132] give a detailed explanation of the cluster-induced smoothing process. Taking the typical case of a Cu_{2000} cluster at 5 eV/atom impinging on a Cu (001) surface they show how, immediately after the impact, a crater is produced by the enormous pressure of 80 GPa at the contact area between cluster and substrate. However, if the cluster impinges on an inclined surface, the crater rim becomes asymmetric: the 'uphill' motion is impeded, while in the 'downhill direction' the crater rim is free to develop. As a result, a net atom transport downhill exists. Since one can consider such an inclined surface as part of a rough surface, the net downhill atom motion serves to decrease the slope and hence the large-scale surface roughness. The same paper shows that good quantitative agreement with corresponding experiments exists.

[133] simulate the smoothing of a fractal rough surface by cluster impact and show that its fractal dimension decreases. [131] study Ar_n impacts ($n = 200 - 1000$) on a Cu target at 20 eV/atom. They show that these cluster impacts reduce surface roughness and propose that this is the effect of atoms sputtered 'sideways' from the cluster, i.e., having a high lateral momentum.

6 Cluster Emission

In the flux of sputtered particles, as a rule not only atoms, but also clusters are found. This applies in particular to the neutral species emitted. Thus in many experiments performed by keV bombardment of metals, a fraction of some 10 % of the sputtered atoms are bound as dimers; therefore quite a large body of information on sputtered dimers has been assembled in the past, and has been reviewed in [152].

The question of how dimers are emitted and what their fraction in the flux of sputtered particles is, has been investigated in several molecular dynamics simulations [23, 153–155]. The results have mostly been interpreted by comparison to the recombination model of cluster formation of *Können* et al. [156, 157].

Shapiro and *Tombrello* [154] study 5 keV Ar impact on Cu (100). They find three main mechanisms for dimer ejection: direct ejection of intact dimers, recombination of two atoms close to the surface (this mechanism has been proposed by *Können* et al. [156, 157]), and so-called 'push-stick' events, in which a cascade atom colliding with a surface atom is ejected together with it in a bound state [158]. At smaller bombarding energies, 300 eV Ar →

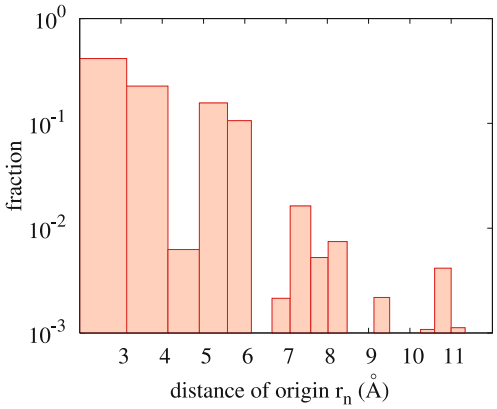

Fig. 4. Distribution of the 'distance of origin' of sputtered dimers: probability that the two atoms contained in a sputtered dimer were at a distance r_n in the solid before emission. Molecular dynamics results [30] for Cu_2 dimers sputtered by 1 keV Ar ions from a Cu target

Cu (100) bombardment, *Karetta* and *Urbassek* [153] find that the majority of sputtered dimers originate from second-nearest neighbour sites, while at higher bombarding energies, above around 1 keV, the majority of dimers stem from nearest-neighbour sites [23, 159]. Figure 4 displays detailed molecular dynamics data of the distribution of the distance that the two atoms contained in the dimer initially had in the target ('distance of origin'). For the specific case of 1 keV Ar → Cu bombardment simulated, some 70 % of the dimers were nearest or second-nearest neighbours in the solid, and have thus been tightly bound to each other before emission. We note that in this simulation the attractive potential extended out to 6.2 Å (5th-nearest-neighbour shell).

Gades and *Urbassek* [155] correlate the dimer sputtering yield Y_2 with the number of sputtered atom pairs, $N_{\mathrm{pairs}} = Y(Y-1)/2$, where Y is the total sputtering yield:

$$Y_2 = p_{\mathrm{clu}} N_{\mathrm{pairs}} \,. \tag{5}$$

Here, the coefficient of proportionality p_{clu} denotes the clustering probability. It assumes a value of around $p_{\mathrm{clu}} = 0.03 - 0.04$ in simulations of 1 keV Cu bombardment of Cu and model Cu alloys. *Gnaser* [47] applies these ideas to experimental data of 1 keV Ar → Cu bombardment and finds his data to be well described by $p_{\mathrm{clu}} = 0.06$, a value comparable to those of the simulations.

A particularly fascinating feature of the sputter phenomenon is that quite large clusters may be emitted. Thus, in experiments of 15 keV Xe bombardment of Ag, Ag clusters up to Ag_{60} have been found [160]; and for the same projectiles bombarding In, even In_{200} has been detected [161]. In these and in

earlier experiments it could be shown that the cluster abundance distribution follows a power-law decay,

$$Y_n \propto n^{-\alpha}\,, \tag{6}$$

and that the exponent α decreases with increasing total sputtering yield. For keV bombardment of Ag, α varies from 8 to 4 [160], for an In target it even reaches the value of 2 [161]; $\alpha = 2$ has also been found by rare-gas-ion bombardment of Au with $400-500\,\mathrm{keV}$ energy, where clusters Au_n with $n > 500$ were detected [162]. A transparent theoretical argument for the origin of the power law (6) is still missing. We note, however, that phenomenological models exist which predict power-law cluster-abundance distributions (6); these are the shock-wave model ($\alpha = 2$) [163] and the thermodynamic-equilibrium model ($\alpha = 7/3$) [164].

Wucher and *Garrison* [165] study sputtering of Ag by up to 5 keV Ar impact. At their highest bombarding energy, the power exponent α reaches a value of 5.3. Good quantitative agreement with experimental data of sputtered-cluster abundance distributions is observed; the authors attribute this fact to the use of a realistic Ag potential [18, 19].

Hartman et al. [166, 167] study cluster emission induced by sputtering of a liquid In-Ga sample by 3 keV Ar impact. The authors investigate the dependence of the cluster yield on the total sputtering yield of the individual ion impact and show a strong positive correlation in the sense that large clusters originate preferably from large-yield events. The power exponent $\alpha = 8.1$ is, however, based only on clusters containing at most 4 atoms. The authors relate their simulation results to a (generalized) recombination model of cluster formation in the spirit of *Können* et al. [156, 157].

In *Colla* et al. [168], simulations of three groups are combined to model the sputtering of a Cu (111) crystal by 5 keV Ar impact and to compare the simulation results to experimental data. Their results exemplify the power-law decay of the cluster-abundance distribution, (6), as shown in Fig. 5. The authors show that large clusters are emitted late after ion impact and originate from 'hot spots', i.e., surface regions with a temperature around or above the melting temperature of copper. A clear correlation of large-cluster emission with the individual sputtering yield could be found such that ion impact events leading to abundant sputtering give also rise to abundant cluster formation.

Muramoto et al. [169] study the cluster formation due to impact of Cu_n clusters on a Cu (111) surface for a cluster energy of 100 eV/atom and for cluster sizes n between 6 and 55. They find the abundance distribution of sputtered clusters to be described by a power law, (6), with an exponent α that decreases with the incident cluster size, and hence with the total sputtering yield. For large sputtering yields α is found to saturate at a value of around 3.

Colla et al. [145, 146] showed that the formation of large clusters (droplets) originating from cluster impact on Au surfaces is connected to the formation

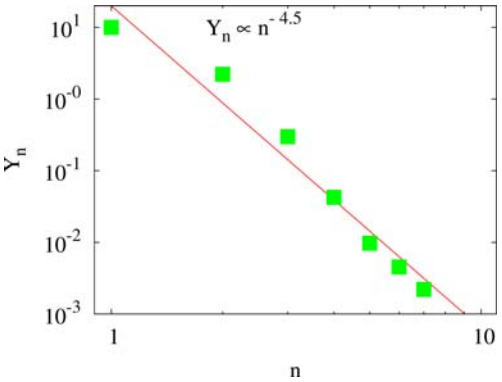

Fig. 5. Abundance distribution of sputtered clusters Y_n vs number of atoms contained in the cluster, n. *Symbols*: Results from molecular dynamics simulations of 5 keV Ar impact on a Cu (111) surface; fragmentation of metastable clusters after emission has been taken into account. *Line*: power-law decay, (6), with $\alpha = 4.5$. Data taken from [168]

of a crater in these events. Large clusters originate from the crater rims; they are emitted comparatively late after ion impact (≥ 10 ps). At this time, the rims are still molten, since they have only poor thermal contact to the bulk of the material. Furthermore, due to the high pressure which initially started the 'micro-explosion' that gave rise to crater formation, the crater rims still contain an outward-directed momentum. It is the balance between the kinetic energy in this outward-directed motion and the potential energy of surface tension that determines whether some part of the crater rim finally is emitted as a large droplet or remains bound to the surface. Figure 6 gives an example of the formation of large clusters late in the sputter process.

As molecular-dynamics simulations show, sputtered clusters as a rule contain a high amount of internal energy. As a consequence, many of them fragent very quickly, on a time scale of 1 ps to several 100 ps, depending on the internal excitation; clusters with an internal excitation just above the dissociation threshold can even live much longer, and can be detected experimentally as metastable clusters on a µs time scale [152]. By calculating the fragmentation process with molecular dynamics, the distribution of stable clusters could be determined. These results were then extrapolated towards larger clusters by a special MC routine built as a post-processor of the molecular-dynamics data; the MC routine incorporates cluster fragmentation via the RRK transition-state theory of unimolecular decay. The result of this simulation shows an astonishingly good overall agreement with the measured data.

Wucher et al. [170] compare experimentally measured and simulated data on the internal energy distributions and fragmentation rate constants of sputtered Fe_n^+ clusters. To this end, the dynamics of the sputtered clusters is followed by molecular-dynamic simulations until 1 ns; the experimental data

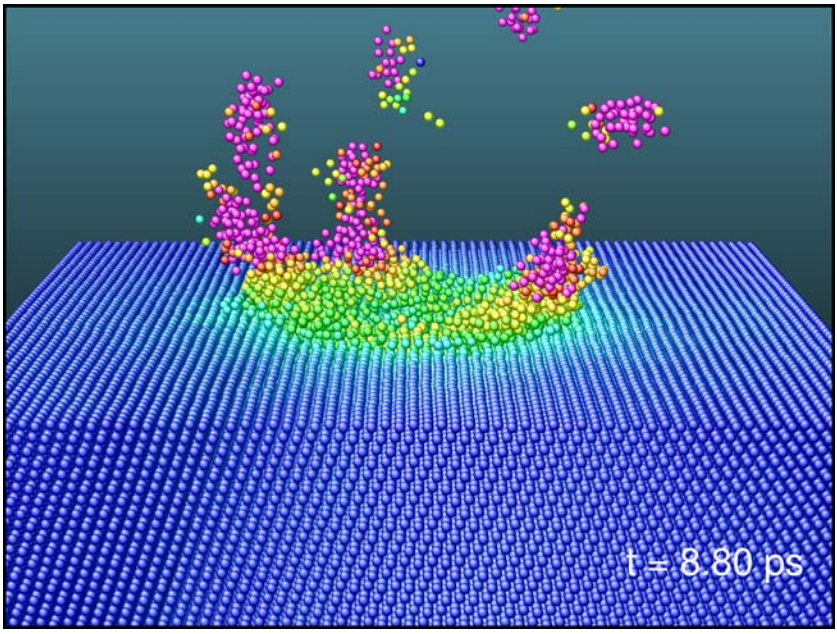

Fig. 6. Perspective view of a Au crystal 8.8 ps after perpendicular impact of a Au_4 cluster with 16 keV total energy on its (111) surface. *Color* denotes local 'temperature'; the *green zone* corresponds to the melting temperature, the *red zone* has reached double this temperature. Data taken from [145]

give information on the time scale of 1 ns and above. The authors obtain fair agreement between measured and simulated internal energies of clusters with sizes between $n = 2$ and 10. The measured internal energies are systematically smaller than the simulated data; the deviation increases with increasing cluster size n and reaches a value of about 50 % for $n = 10$. This deviation is discussed to be due to further ongoing evaporation and fragmentation processes occurring in the sputtered clusters after the end of the simulation time, 1 ns. The authors derive information on the fragmentation rates from their data and the comparison between simulation and experiment.

Another feature which has already been studied in some detail by molecular dynamics in the past was molecule sputtering; i.e., the emission of preformed molecules from the surface. Sputtering of adsorbed molecules and their fragmentation were investigated in [171, 172].

7 Surface Topography Formation

The energy deposited by the irradiating particle close to the surface leads, besides sputtering, to the formation of a variety of surface defects: isolated

adatoms and surface vacancies, and their clustered analogues, i.e., adatom islands and surface-vacancy islands. In extreme cases considerable craters may be created, with adjacent crater rims consisting of piled-up adatoms.

7.1 Surface Vacancy and Adatom Production

These phenomena are directly related, and relevant, to the sputtering process: 1. Adatoms may be viewed as atoms which have attempted to be ejected from the surface, but have not succeeded since their kinetic energy was too small with respect to the surface binding energy. 2. Due to the formation of surface topography, the next impinging ion will encounter an altered surface, and hence the sputtering behaviour may be changed.

The creation of adatoms on a surface induced by keV-atom impact has first been observed by *Harrison* and *Webb* in molecular-dynamics simulations [12, 173, 174].

Ghaly et al. [175] present an extended study of surface damage produced by $5 - 20\,\mathrm{keV}$ self-ion bombardment in several metals and germanium. They identify three separate mechanisms:

1. ballistic damage created in the linear collision cascade
2. viscous flow due to local melting and the forced flow of liquid to the surface
3. micro-explosions induced by the high pressure in the cascade which lead to rupturing the nearby surface.

Gades and *Urbassek* [176] investigated the formation of adatoms on the Pt (111) surface, induced by the impact of rare-gas atoms with energies below 3 keV. For not too small bombarding energies, $> 200\,\mathrm{eV}$, they found for the ratio of the adatom yield Y_a to the sputtering yield Y_s:

$$Y_\mathrm{a}/Y_\mathrm{s} \cong 4\,, \tag{7}$$

in agreement with a simple model derived from analytical sputter theory [176]. This ratio is quite independent of the projectile species. For lower bombarding energies, the number of adatoms formed increases strongly with respect to the sputtering yield, cf. Fig. 7.

In later work, *Busse* et al. [177] investigated adatom production on the Al (111) surface and compared to experimental measurements. Excessive adatom production was found which leads to an experimentally observable irradiation-induced growth instead of the expected erosion for keV Xe impact. In contrast to the Pt (111) surface, the low melting temperature of aluminium emphasises the role of the molten zone induced by the ion impact. Rapid resolidification leaves amorphous parts in the bulk, thus separating surface adatoms from the bulk vacancies and inducing swelling.

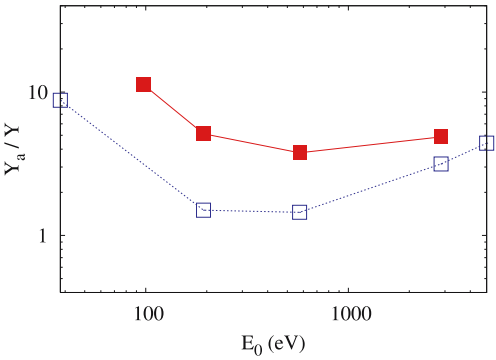

Fig. 7. Ratio of the yield of adatoms, Y_a, to the sputtering yield Y for Xe ion bombardment of a Pt (111) surface. *Open symbols*: molecular-dynamics simulation. *Full symbols*: experimental data. Lines to guide the eye. Data taken from [176]

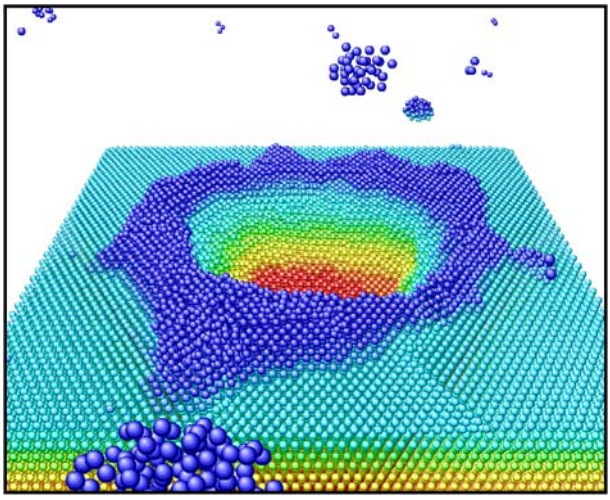

Fig. 8. Perspective view of the crater formed in a Au (111) crystal 40 ps after bombardment with a 64 keV Au_4 cluster. *Color* denotes height above the surface. Data taken from [146]

7.2 Crater Production

Ion bombardment may lead to individual craters at the surface. This phenomenon is quite ubiquitous in cases where a strong thermal spike is formed [178]. In [179], as well as in [180] and also earlier in [181], cratering induced by ions and small clusters is connected to cratering processes induced by hypervelocity projectiles, such as cosmic dust particle or meteorites. Figure 8 presents a view of a crater formed by the sputter process.

Aderjan and *Urbassek* [179] discussed crater formation by Cu_n clusters ($n = 13, 43$) impinging with total energies between 5 and 20 keV on a Cu (100) surface. They find craters to be formed above the threshold bombarding energy of around 5 keV. Then the crater volume increases linearly with the bombarding energy. By artificially varying the cohesive energy of their target, they find that the crater volume scales inversely proportional to the *square* of the target cohesive energy.

Nordlund et al. [182] re-investigate the dependence of the size of ion-induced craters on the materials properties of the target. For this end, they change parameters of the target-target atom interaction potential. In this way they show that the crater size scales inversely proportional to the cohesive energy and to the melting temperature of the material.

Bringa et al. [178] studied this phenomenon by considering Xe impacts on Au for energies between 0.4 and 100 keV. They find that in a low-energy regime (< 10 keV), the mechanism can be understood by considering the high energy density deposited by the projectile in the vicinity of the surface. They argue that at high impact energies (> 50 keV), the formation of craters can be attributed to the long lifetime of the induced heat spike.

Nordlund et al. [183] identify various macroscopic features connected to crater production by < 100 keV atom and cluster impact on heavy metals (Ag and Au). Similarly as in experiment [184, 185], they find the craters produced to be often of a highly asymmetric form, accompanied by adatom ridges extending far from the crater itself. The origin of these structures is reported to lie in atomic 'fingers' and 'bridges', which exist above the crater structure; these structures are propelled onto the surface, resulting in the features observed.

Bringa et al. investigate crater formation by fast-ion impact in the electronic stopping regime [186, 187]. They find the threshold for crater formation to occur when the excitation density in the ion track approaches the cohesive energy density; indexcohesive energy a crater rim is formed at about 6 times that energy density. The crater length scales roughly as the square root of the electronic stopping power, and the crater width and depth seem to saturate for the largest energy densities considered. They also find the crater to be much larger than expected from the sputtering yield, and argue therefore that the crater size cannot easily be used to estimate the sputtering yield.

8 Effects of Surface Topography on Sputtering

In molecular-dynamics computer simulation, as a rule, sputtering onto a flat surface is considered. However, in experiment the surface is usually rough. Various forms of surface topography can be found on real surfaces: Atomic-scale roughness, surface steps, larger-scale structures like ripples etc.

The sputtering of surfaces with a large-scale topography, such as ripples, can be easily described, as long as the spatial extent of the collision cascade

is small compared to the curvature radius of the surface structure. Then, the main influence of the surface topography is to alter the incidence angle of the bombarding ion with respect to the local surface normal. In principle, also the surface curvature may influence the sputtering yield. The incorporation of such effects is well possible within analytical sputter theory [188, 189] and does not require modelling on a molecular-dynamics basis. Note, however, the study by *Moseler* et al. [132] discussed in Sect. 5.2.3 on surface smoothing of a rippled surface by cluster beams.

Atomistically rough surfaces, on the other hand, are well suited for a study by molecular-dynamics simulation. In one particular study [190], a Pt (111) surface was randomly covered with a definite coverage Θ of adatoms. Only a small effect, of the order of 10 %, on the sputtering yield was observed. This is reassuring in view of the fact that sputter theory employs a mean, site-independent value for the surface binding. In an earlier simulation [191], analogous results were obtained for pair-potential interaction and a surface covered with half a monolayer of adatoms.

The formation of surface topographical structures may affect the sputtering behavior of the surface. In craters, for instance, redeposition will act to lower the sputtering yield. Due to the general dependence of the sputtering yield on the incidence angle of the bombarding ion, any large-scale (i.e., on the length of a cascade dimension) surface structure will change the incidence angle of the bombarding ion with respect to the local surface normal. Calculations of the consequences of this feature on surface topography formation have been performed [188, 189], but not on a molecular-dynamics basis.

In the case of covalent materials with their directional bonding, the effect of surface topography may be considerably stronger. A detailed study of the effect of 225 eV Xe bombardment on the surface topography evolution of Si(111) and the influence of this topography on the sputtering mechanism has been performed in [192]; the results were shown to be consistent with the layer-by-layer sputter mode found in experiment [193].

8.1 Effect of Surface Steps on Sputtering

A basic irregularity occurring on crystalline surfaces are steps. These occur necessarily in a quite regular fashion on vicinal surfaces, i.e., surfaces that are cut under a small angle towards a low-indexed surface. Furthermore, steps form the boundary between adatom islands or vacancy islands on an otherwise flat terrace. Thus steps form an essential structure occurring on realistic surfaces.

With the advent of high-resolution surface-topography measurement techniques, such as in particular the scanning tunnelling microscope, the ion-induced damage on a surface can be directly observed. Using low fluences, the damage induced by individual ions can be observed experimentally. Including experimental knowledge on the diffusion behaviour of defects, such measurements also allow to deduce the individual sputtering yield from such

measurements. Thus, recently, molecular-dynamics investigations of sputtering of ions interacting with surface steps have been reported.

Early work on the application of molecular-dynamics simulation on stepped surfaces was concerned with ion-induced defect formation and interlayer mobility close to steps. Thus *Mazzone* [194] studied the effects of a primary knock-on atom (PKA) with energies below 10 eV in the vicinity of a step on a Si (100) surface, where the possiblilty of sputtering is also explored. In [195] this study is extended to low-energy ($5 - 30$ eV) irradiation by Ar and B atoms, where the effect of a step on the implantation and reflection probability is investigated. *Jacobsen* et al. [196] use molecular-dynamics simulation to study the energetic beam deposition of Ag → Ag (111), and Pt → Pt (111), for incoming energies up to 35 eV. They inquire in particular into the dependence of the impact-induced interlayer mobility as a function of the impact distance to a step on the surface.

Shapiro and *Tombrello* [197] study the impact of 5 keV Ar → Cu (111) surface in the vicinity of a step and compare to the values for a flat terrace. These authors restrict their bombarding angle to polar angles $\theta < 50°$ with respect to the surface normal. Around the surface normal, $\theta < 30°$, a slight reduction in the sputtering yield is found, while for $\theta > 30°$, the sputtering yield exceeds that of a flat terrace.

Friedrich and *Urbassek* [198] study more oblique and even glancing incidence angles for 5 keV Xe impact on a stepped Pt (111) surface. The sputtering yield shows a maximum around $\theta = 60°$ similar to ion impact on a flat (111) terrace; the influence of the existence of a step on the surface on the sputtering yield is in the 20 % range. For more glancing incidence, however, the presence of a step increases the sputtering yield dramatically. Thus, e.g., for 80° incidence angle, the sputtering yield from a flat terrace is 0 while it amounts to 20 if the ion impinges in the vicinity of a step. In the molecular-dynamics simulation, the influence of the exact ion impact point in the vicinity of the step could be explored. It was shown that the effect is maximum if the ion impinges on the lower terrace in front of the step with a direction towards the step, and the range of influence of the step on the yield could be determined and rationalized by a simple geometrical model. Figure 9a exemplifies the considerable sputtering induced by 5 keV Ar impact on a terraced Pt (111) surface at 83° incidence towards the surface normal. Note that for this impact angle, on a flat terrace the sputtering yield is almost zero. In a recent publication [199] such molecular-dynamics simulation data could be used to interprete experimental data on the fluence dependence of sputtering of Pt (111), where with increasing fluence the number of islands, and thus the effective step length, changes and influences the sputtering yield. Figure 9b exemplifies the change in surface topography induced by glancing-incidence keV-ion impact in the vicinity of a surface step.

Karolewski [200] studies 3 keV glancing Ar ion incidence on a stepped Cu (100) surface and shows that sputtered atoms originate preferentially from the vicinity of the steps.

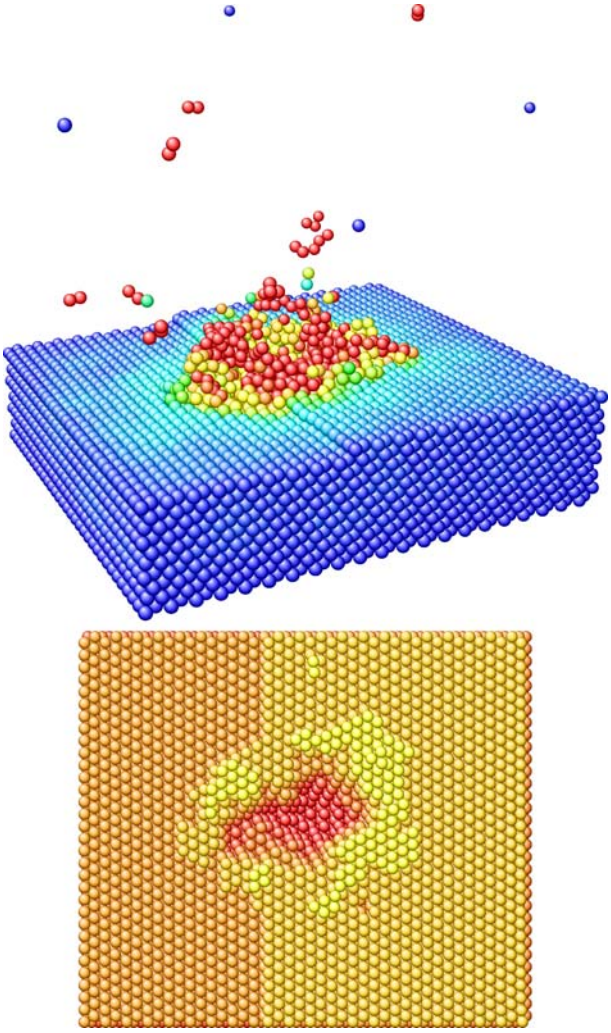

Fig. 9. Sputtering of a terraced Pt (111) surface induced by a 5 keV Ar ion. The ion impinges at an angle of $\theta_0 = 83°$ towards the surface normal onto the lower terrace from the left in the direction of the ascending step. **a**) Perspective view at 2.5 ps after impact. *Color* denotes local 'temperature'; the *red zone* corresponds to the melting temperature. **b**) *Top view* of the damaged surface at 20 ps after impact. *Color* denotes height above the surface

9 Fluence Dependence of Sputtering

Solids change during the irradiation with energetic projectiles. This has several reasons:

1. Erosion (sputtering) changes the surface topography; thus surfaces may become atomically rough. They may also develop surface topography such as craters with adatom rims, or surface vacancy and adatom islands. After higher fluences, also mesoscopic structures may be formed such as ripples or nano-dots.
2. Furthermore, in the case of non-selfbombardment, the incorporation of the bombarding atoms into the surface will change the surface composition, and hence the sputtering behaviour.
3. In the case of a non-elemental target, further composition changes are brought about by preferential sputtering effects.

The molecular-dynamic simulation of fluence effects on sputtering is primarily hampered by the different time scales which enter this problem. While individual ion-induced processes, and hence sputtering, occur after 100 ps at most after ion impact, the advent of the next ion impinging on the same relevant surface area ($10-100\,\mathrm{nm}^2$, say) will occur after microseconds or seconds, depending on the ion current density. Finally, the entire sputter experiment may take minutes or hours until completion. Clearly such time scales are completely inaccessible to a molecular-dynamics treatment. Several hybrid approaches, combining molecular-dynamics techniques to describe the individual ion-induced phenomena with (kinetic) Monte Carlo simulations for assessing the phenomena occurring in between the individual ion impacts, have been devised, in particular in the areas of energetic beam deposition and thin-film growth processes [196, 201, 202].

However, several investigations on the fluence dependence of sputtering have also appeared which are purely based on molecular dynamics. This means that the activity of all processes occurring in between the individual ion impacts has been neglected. This approach thus describes the zero-temperature limit of dynamic sputtering: The substrate temperature must be so small that any atom migration is suppressed, at least at and in the vicinity of the surface.

Si (100) amorphisation under Ar bombardment was investigated by *Marqués* et al. [26, 203, 204] and by *Haddeman* and *Thijsse* [205]. *Zhong* et al. [206] investigated the ion-beam-induced smoothing of metal surfaces by 40 keV Xe ion impact. *Hanson* et al. [207] present a study of selfsputtering of nickel and aluminium (111) surfaces by low-energy projectiles. *Peltolta* et al. [208] study the fluence dependence of range profiles in Si. Most recently, *Karolewski* [209] investigates the sputtering of a Cu (100) crystallite surface by 2 keV copper ions up to a fluence of $1.25 \times 10^{14}\ \mathrm{cm}^{-2}$. He finds a broadening of the angular distribution and a rapid increase of the depth of origin of sputtered atoms. Both effects originate from the surface roughening induced

by sputtering on the copper surface. Other sputtered-particle properties such as the sputtering yield, and the sputtered-atom energy distribution, are quite insensitive to fluence.

10 Sputtering of Molecular and Organic Solids

The understanding of sputtering of molecular solids is of importance in a variety of applications ranging from SIMS of organic materials to desorption processes in matrix isolation spectroscopy. Also the sputtering of ice-covered surfaces, such as the moons in the outer solar system, comets or particles constituting the rings of the giant planets, provide motivation for studying ion-induced processes and sputtering in molecular solids. The simulation of these processes with molecular dynamics requires – besides the knowledge of the role that target electrons, which may become excited during ion bombardment, play for the ensuing processes – an understanding of the interatomic and intermolecular interaction potentials in these solids. Since in the last decade the description of these potentials has matured, more and more computer simulations of these systems have been performed.

10.1 Diatomic and Small Anorganic Molecular Solids

Diatomic molecular solids like O_2 and N_2 have been investigated in a variety of studies. Here simulations have been performed using site-site potentials in which each atom interacts with the other atoms in neighbouring molecules via a pair potential (typically the Lennard-Jones potential), while the intramolecular interaction is simulated by a Morse potential. This allows for vibrational and rotational excitation of the molecules and also dissociation. Recombination of dissociated atoms and further reactions have generally been excluded from consideration.

In an early study, *Kafemann* and *Urbassek* [210] investigated the sputtering of a condensed N_2 sample by 100 eV N atom impact. The temporal evolution of the heat spike in the sample, and of the sputtering, are investigated and data for the kinetic energy distribution of sputtered molecules as well as the partitioning of the sputtered energy into translational, rotational and vibrational energy are given in this case study.

The sputtering of other inorganic solids or ices has been studied only rarely using molecular dynamics. An exception is [211] where water ice has been modelled induced by O^+ ions at energies between 23 and 115 eV. Energy and angular distributions of ejected H_2O molecules are described and the emission of $(H_2O)_n$ clusters is reported.

Several simulations were performed that mainly aimed at understanding the electronic sputtering of molecular solids, induced by MeV light ions [106, 109, 212]. Vibrational and rotational excitation as well as dissociation were studied, and the dependence of the sputtering yield on the energy deposited

by the fast projectile in the ion track were investigated. In earlier studies, the vibrational to translational coupling of diatomic molecular model crystals was investigated [32, 213–216], where a reduced intramolecular well depth was employed to enhance the coupling.

10.2 Sputtering of Organic Solids

The sputtering of solids – or overlayer films – consisting of organic molecules, e.g., hydrocarbons, polymers, or more complex organic materials – has attracted considerable interest in the recent past, in particular due to applications in organic SIMS. Several reviews have been dedicated to the molecular-dynamic simulation of these events [217, 218].

Very early studies modelled organic molecules as single entities, in the sense of (soft) spheres and a simple intermolecular interaction potential [102]. While these early studies do not allow for molecule fragmentation and not even for internal excitation, the breathing sphere approach – which has been extensively used for studying laser ablation of organic films [219,220] – aims at including internal excitation via one internal degree of freedom, the breathing mode. Clearly, energetic atom irradiation may create more extensive internal excitation, and molecule fragmentation and dissociation, such that more refined interaction potentials need to be used to model the internal degrees of freedom. Ideally they also allow for the inclusion of reaction processes of the radicals created by ion bombardment. This has become possible through the invention of sophisticated classical interaction potentials of which we mention the hydrocarbon potential developed by *Brenner* [221, 222] and the AIREBO potential by *Stuart* and *Harrison* [223]. This potential allows to improve the inter-molecular interaction while still maintaining the reactive nature of the potential. The latter potential has been used recently in [224,225] for studying the sputtering of benzene molecular crystals and multilayer films adsorbed on Ag (111) by 0.3 keV Xe and 4 keV Ar projectiles, respectively.

The following features in the sputtering of organic solids were demonstrated in the simulations:

- Formation of fragments.
- Reactions between fragments (radical-radical recombinations).
- Molecule emission by a collective mechanism called ‘molecule liftoff’ [217].
- Individual high-yield events have been reported and analyzed [226].
- Quantitative results on energy and angular distributions, e.g., for benzene molecules desorbed from the surface of a Ag (111) surface, have been reported [227].

10.3 Sputtering of Polymers

These simulations have also been extended to study the sputtering of polymers. The work of *Beardmore* and *Smith* on the ion bombardment of

polyethylene [228] gives an early example. More recently, *Delcorte* and co-workers [229] reported on simulations of the particle-induced fragmentation and sputtering of a 7.5 kDalton organic sample based on a polystyrene coil adsorbed on Ag (111). Using the AIREBO potential, the emission of recombined and rearranged fragments is reported, the existence of long-lived vibration excitations is demonstrated and delayed emission via vibration-induced bond scission is observed.

11 Chemical Effects

While chemical effects, i.e., reactions, may play some role in any bombardment of a non-elemental solid in which the two species present are not completely chemically inert, and in particular in the bombardment of molecular and organic samples, the term 'chemical sputtering' implies that the chemistry induced in the sample by the irradiation, and in particular by reactions between the projectile and target atoms, contributes by itself significantly to the sputter process. Chemical effects can only be modelled if potentials are available which include the chemistry at least in a qualitative way [230]. A prominent example of such a potential is the so-called Brenner potential [221, 222], an example of the class of bond-order potentials [231], which has been found to describe well the chemistry of hydrocarbons.

Nordlund et al. [232–234] describe the low-energy (< 100 eV) sputtering of an amorphous hydrogenated carbon (a-C:H) target by H atoms. By using the Brenner potential [221, 222], they allow for the inclusion of reactions in the simulation. Erosion yields far exceeding those expected for a physical sputtering process are observed in the simulation. This is attributed to a process termed 'swift chemical sputtering' by a C-C bond-breaking mechanism induced by the swift H ions.

The sputtering or reactive ion beam etching (RIBE) of Si by F and Cl has been investigated by *Garrison* and co-workers [235, 236] and by *Feil* [237]; these studies became possible after the availability of potentials for thermal surface reactions – such as the thermal etching of a Si surface by F atoms – was demonstrated [238]. The system studied was 200 eV Ar bombardment of Si in a Cl atmosphere. The simulations were used to interprete the synergetics of chemical sputtering, and the emission mechanisms of low-energy reaction products. In other work, the sputtering of a H-terminated Si-surface by low-energy ion irradiation was studied [239].

A possible pathway for Si etching was demonstrated to be the breaking of a Si-Si bond by an incoming F atom. *Barone* and *Graves* [240, 241] modelled Si sputtering by F or Cl atoms with energies between 10 and 50 eV, and also the sputtering of fluorinated Si samples by low-energy Ar atoms [242]. The potentials used are based on the Stillinger-Weber potential [243]. These authors also performed 'high fluence' simulations, in which the transformation of the original Si to a $SiCl_x$ layer was observed. Cl incorporation, Si etching

and the resulting surface roughness are reported. These simulations were extended by *Abrams* and *Graves* [244] to Si etching by energetic (100 eV) CF_3^+ bombardment.

Chiba et al. [245] study low-energy (< 30 eV) F etching of Si and emphasize the effect of the substrate temperature and the ion incidence angle. *Aoki* et al. [246] extend these studies to etching of Si by F cluster impact with clusters containing up to 6000 atoms.

12 Conclusions

The strength of the molecular-dynamics method is based on the simple physical picture behind it – the solution of Newton's equations of motion – and the small number of physical input required: The interatomic interaction potential, and (when appropriate) the coupling of the atoms to the electrons. In this sense, it is simple to judge whether a given application has been modelled adequately by a simulation.

In the actual implementation, besides these questions a number of more technical (or numerical) issues need be solved: System size and the connected question of the boundary conditions of the simulation cell, the duration of the simulation, and the question of sufficient statistics – usually the answer to a physical question is the average over many simulations in which the initial conditions are slightly varied.

Often molecular-dynamics simulations are undertaken in order to obtain insight on mechanisms at work in sputtering, to obtain a qualitative picture of the event, and to study exemplary cases. Here, the benefit of this atomistic simulation method to lend itself easily to visualization is often exploited. Nowadays the production of animated video sequences has become routine and helps to convey insight into the dynamics of the sputter processes investigated. However, in several of the research results presented in this chapter, it became also apparent that molecular-dynamics simulation is in selected research issues equally well suited to provide systematic information and quantitative results. Such studies include those on preferential sputtering of isotope systems, sputtering by cluster impact, or the influence of surface topography on the sputtering yield.

The research fields in which molecular dynamics is best applied are those, where simpler or faster methods, such as analytical theory, Monte-Carlo and BCA simulation, fail or where their assumptions need to be controlled. These include issues,

1. where many-body interactions are essential, such as sputtering from high-energy-density zones (spikes) or sputtering by cluster impact;
2. which are controlled by collective motion, such as cluster emission, the formation of surface topography and, in particular, craters;

3. where the bonding situation is complex, such as in molecular and organic targets, in compounds, in chemical sputtering and also for rough surfaces.

However, this method will also be used at advantage in those areas where the assumptions entering other simulation procedures or analytical theory need to be controlled by a more realistic simulation. This includes the areas of isotope sputtering, the effect of surface topography on sputtering, and the fluence dependence of sputtering.

Acknowledgements

Thanks are due to C. Anders, C. Engin, Y. Rosandi, and St. Zimmermann for help with the preparation of the figures.

References

[1] R. Behrisch (Ed.): *Sputtering by Particle Bombardment I*, Top. Appl. Phys. **47** (Springer, Berlin, Heidelberg 1981) russ. translation: (MIR, Moscow 1984) 189
[2] R. Behrisch (Ed.): *Sputtering by Particle Bombardment II*, Top. Appl. Phys. **52** (Springer, Berlin, Heidelberg 1983) russ. translation: (MIR, Moscow 1986) 189
[3] R. Behrisch, K. Wittmaack (Eds.): *Sputtering by Particle Bombardment III*, Top. Appl. Phys. **64** (Springer, Berlin, Heidelberg 1991) russ. translation: (MIR, Moscow 1998) 189
[4] P. Sigmund (Ed.): *Fundamental Processes in Sputtering of Atoms and Molecules (SPUT92)*, K. Dan. Vidensk. Selsk. Mat. Fys. Medd. **43** (1993) 189
[5] P. Sigmund: Phys. Rev. **184**, 383 (1969) 189
[6] J. P. Biersack, W. Eckstein: Appl. Phys. A **34**, 73 (1984) 189
[7] M. T. Robinson, I. M. Torrens: Phys. Rev. **9**, 5008 (1974) 189
[8] W. Eckstein: *Computer Simulation of Ion-Solid Interactions*, Springer Ser. Mater. Sci. **10** (Springer, Berlin, Heidelberg 1991) russ. translation: (MIR, Moscow 1995) 189, 190
[9] J. B. Gibson, A. N. Goland, M. Milgram, G. H. Vineyard: Phys. Rev. **120**, 1229 (1960) 189
[10] B. J. Alder, T. E. Wainwright: J. Chem. Phys. **27**, 1208 (1957) 189
[11] H. H. Andersen: Nucl. Instrum. Methods B **18**, 321 (1987) 190
[12] D. E. Harrison, Jr.: Crit. Rev. Solid State Mater. Sci. **14**, S1 (1988) 190, 209
[13] M. T. Robinson: K. Dan. Vidensk. Selsk. Mat. Fys. Medd. **43**, 27 (1993) 190
[14] R. M. Nieminen: K. Dan. Vidensk. Selsk. Mat. Fys. Medd. **43**, 81 (1993) 190, 200
[15] H. M. Urbassek: Nucl. Instrum. Methods B **122**, 427 (1997) 190
[16] R. Smith (Ed.): *Atomic and ion collisions in solids and at surfaces* (Cambridge Univ. Press, Cambridge 1997) 190
[17] N. Winograd: Mat. Fys. Medd. Dan. Vid. Selsk. **43**, 223 (1993) 191

[18] T. J. Raeker, A. E. DePristo: Int. Rev. Phys. Chem. **10**, 1 (1991) 191, 206
[19] M. S. Stave, D. E. Sanders, T. J. Raeker, A. E. DePristo: J. Chem. Phys. **93**, 4413 (1990) 191, 206
[20] R. Maboudian, Z. Postawa, M. El-Maazawi, B. J. Garrison, N. Winograd: Phys. Rev. B **42**, 7311 (1990) 191
[21] S. W. Rosencrance, J. S. Burnham, D. E. Sanders, C. He, B. J. Garrison, N. Winograd, Z. Postawa, A. E. DePristo: Phys. Rev. B **52**, 6006 (1995) 191
[22] K. Johannessen: Nucl. Instrum. Methods B **71**, 171 (1992) 191
[23] G. Betz, R. Kirchner, W. Husinsky, F. Rüdenauer, H. M. Urbassek: Radiat. Eff. Defects Solids **130–131**, 251 (1994) 192, 204, 205
[24] S. W. Rosencrance, N. Winograd, B. J. Garrison, Z. Postawa: Phys. Rev. B **53**, 2378 (1996) 192
[25] H. Gades, H. M. Urbassek: Appl. Phys. A **61**, 39 (1995) 192, 193
[26] J. E. Rubio, L. A. Marqués, M. Jaraíz, L. A. Bailón, J. Barbolla: Nucl. Instrum. Methods B **102**, 301 (1995) 192, 215
[27] R. Smith, D. E. Harrison, Jr., B. J. Garrison: Phys. Rev. B **40**, 93 (1989) 192
[28] R. A. Stansfield, K. Broomfield, D. C. Clary: Phys. Rev. B **39**, 7680 (1989) 192
[29] V. I. Shulga, W. Eckstein: Nucl. Instrum. Methods B **145**, 492 (1998) 192
[30] T. J. Colla, H. M. Urbassek: Nucl. Instrum. Methods B **152**, 459 (1999) 192, 205
[31] R. E. Johnson, J. Schou: K. Dan. Vidensk. Selsk. Mat. Fys. Medd. **43**, 403 (1993) 192
[32] R. E. Johnson, M. Liu: J. Chem. Phys. **104**, 6041 (1996) 192, 217
[33] P. Klein, H. M. Urbassek, M. Vicanek: Phys. Rev. B **51**, 4597 (1995) 192
[34] J. D. Kress, D. E. Hanson, A. F. Voter, C. L. Liu, X. Y. Liu, D. G. Coronell: J. Vac. Sci. Technol. A **17**, 2819 (1999) 193
[35] H. Coufal, H. F. Winters, H. L. Bay, W. Eckstein: Phys. Rev. B **B44**, 4747 (1991) 193
[36] H. L. Bay, H. F. Winters, H. J. Coufal, W. Eckstein: Appl. Phys. A **55**, 274 (1992) 193
[37] C. F. Abrams, D. B. Graves: J. Appl. Phys. **86**, 2263 (1999) 193
[38] C. F. Abrams, D. B. Graves: IEEE Trans. Plasma Sci. **27**, 1426 (1999) 193
[39] C. Steinbrüchel: Appl. Phys. Lett. **55**, 1960 (1989) 193
[40] C. F. Abrams, D. B. Graves: J. Vac. Sci. Technol. A **16**, 3006 (1998) 193
[41] A. Kubota, D. J. Economou: IEEE Trans. Plasma Sci. **27**, 1416 (1999) 193
[42] M. H. Shapiro, E. Trovato, T. A. Tombrello: Nucl. Instrum. Methods B **180**, 58 (2001) 193
[43] Z. B. Güvenc, Y. Hundur, R. Hippler: Nucl. Instrum. Methods B **164-165**, 854 (2000) 193
[44] R. V. Stuart, G. K. Wehner: J. Appl. Phys. **33**, 2345 (1962) 193
[45] P. Sigmund, N. Q. Lam: K. Dan. Vidensk. Selsk. Mat. Fys. Medd. **43**, 255 (1993) 193
[46] P. Sigmund: in R. Behrisch (Ed.): *Sputtering by Particle Bombardment I*, Top. Appl. Phys. **47** (Springer, Berlin, Heidelberg 1981) p. 9 194, 198
[47] H. Gnaser: *Low-Energy Ion Irradiation of Solid Surfaces*, Tr. Mod. Phys. **146** (Springer, Berlin, Heidelberg 1999) 194, 205
[48] H. Gades, H. M. Urbassek: Nucl. Instrum. Methods B **102**, 261 (1995) 194, 195

[49] M. H. Shapiro, P. K. Haff, T. A. Tombrello, D. E. Harrison, Jr.: Nucl. Instrum. Methods B **12**, 137 (1985) 194
[50] M. H. Shapiro, T. A. Tombrello, D. E. Harrison, Jr.: Nucl. Instrum. Methods B **30**, 152 (1988) 194
[51] D. Y. Lo, T. A. Tombrello, M. H. Shapiro: Nucl. Instrum. Methods B **40/41**, 270 (1989) 194
[52] N. Q. Lam, K. Johannessen: Nucl. Instrum. Methods B **71**, 371 (1992) 195
[53] V. I. Shulga, P. Sigmund: Nucl. Instrum. Methods B **103**, 383 (1995) 195
[54] V. I. Shulga, P. Sigmund: Nucl. Instrum. Methods B **119**, 359 (1996) 195
[55] R. Behrisch: in R. Behrisch (Ed.): *Sputtering by Particle Bombardment II*, Top. Appl. Phys. **52** (Springer, Berlin, Heidelberg 1983) p. 1 196
[56] M. Szymonski: K. Dan. Vidensk. Selsk. Mat. Fys. Medd. Dan. **43**, 495 (1993) 196
[57] E. M. Bringa, R. E. Johnson: Phys. Rev. Lett. **88**, 165501 (2002) 196, 201
[58] Y. S. Dou, L. V. Zhigilei, N. Winograd, B. J. Garrison: J. Phys. Chem. A **105**, 2748 (2001) 196
[59] K. Nordlund: Nucl. Instrum. Methods B **218**, 9 (2004) 196
[60] C. Liu, et al.: Nucl. Instrum. Methods B **178**, 200 (2001) 196
[61] W. Jiang, W. J. Weber, S. Thevuthasan: J. Appl. Phys. **87**, 7671 (2000) 196
[62] D. Ramasavmy, S. D. Kenny, R. Smith: Nucl. Instrum. Methods B **202**, 175 (2003) 196
[63] D. A. Young: Europhys. Lett. **59**, 540 (2002) 196
[64] D. A. Young: Nucl. Instrum. Methods B **225**, 231 (2004) 196
[65] M. H. Shapiro, T. A. Tombrello: Nucl. Instrum. Methods B **90**, 473 (1994) 197
[66] M. H. Shapiro, T. A. Tombrello: Nucl. Instrum. Methods B **94**, 186 (1994) 197
[67] M. H. Shapiro, T. A. Tombrello: Nucl. Instrum. Methods B **102**, 277 (1995) 197
[68] M. H. Shapiro, T. A. Tombrello: Nucl. Instrum. Methods B **66**, 317 (1992) 197
[69] J. Lindhard, M. Scharff: Phys. Rev. **124**, 128 (1961) 197
[70] O. B. Firsov: Sov. Phys. JETP **36**, 1076 (1959) 197
[71] I. S. Tilinin: Phys. Rev. A **51**, 3058 (1995) 197
[72] P. M. Echenique, R. M. Nieminen, J. C. Ashley, R. H. Ritchie: Phys. Rev. A **33**, 897 (1986) 197
[73] A. Caro: Radiat. Eff. Defects Solids **130-131**, 187 (1994) 197, 200
[74] S. Prönnecke, A. Caro, M. Victoria, T. Diaz de la Rubia, M. W. Guinan: J. Mater. Res. **6**, 483 (1991) 197
[75] V. G. Kapinos, D. J. Bacon: Phys. Rev. B **50**, 13194 (1994) 197
[76] K. Nordlund, L. Wei, Y. Zhong, R. S. Averback: Phys. Rev. B **57**, R13965 (1998) 197
[77] I. Koponen: J. Appl. Phys. **72**, 1194 (1992) 197, 200
[78] I. Koponen: Phys. Rev. B **47**, 14011 (1993) 197
[79] S. Meyer, D. Diesing, A. Wucher: Phys. Rev. Lett. **93**, 137601 (2004) 197
[80] M. H. Shapiro, J. Fine: Nucl. Instrum. Methods B **44**, 43 (1989) 197
[81] D. N. Bernardo, B. J. Garrison: J. Chem. Phys. **97**, 6910 (1992) 197
[82] M. H. Shapiro, T. A. Tombrello, J. Fine: Nucl. Instrum. Methods B **74**, 385 (1993) 197

[83] I. Wojciechowski, B. J. Garrison: Surf. Sci. **527**, 209 (2003) 197
[84] Z. Sroubek, F. Sroubek, A. Wucher, J. A. Yarmoff: Phys. Rev. B **68**, 115426 (2003) 197
[85] C. P. Flynn, R. S. Averback: Phys. Rev. B **38**, 7118 (1988) 197, 198, 200
[86] M. W. Finnis, P. Agnew, A. J. E. Foreman: Phys. Rev. B **44**, 567 (1991) 197, 200
[87] I. Koponen, M. Hautala: Nucl. Instrum. Methods B **93**, 374 (1994) 197, 200
[88] A. Caro, M. Victoria: Phys. Rev. A **40**, 2287 (1989) 197, 200
[89] D. E. Harrison, Jr., M. M. Jakas: Nucl. Instrum. Methods B **15**, 25 (1986) 198
[90] Z. Sroubek: Nucl. Instrum. Methods B **78**, 140 (1993) 198
[91] A. Wucher, Z. Sroubek: Phys. Rev. B **55**, 780 (1997) 198
[92] A. Duvenbeck, Z. Sroubek, F. Sroubek, A. Wucher: Nucl. Instrum. Methods B **225**, 464 (2004) 198
[93] H. L. Bay, H. H. Andersen, W. O. Hofer, O. Nielsen: Nucl. Instr. Methods **132**, 301 (1976) 198
[94] H. H. Andersen: K. Dan. Vidensk. Selsk. Mat. Fys. Medd. **43**, 127 (1993) 198, 202
[95] M. Ghaly, R. S. Averback: Phys. Rev. Lett. **72**, 364 (1994) 198
[96] H. M. Urbassek, K. T. Waldeer: Phys. Rev. Lett. **67**, 105 (1991) 198
[97] K. T. Waldeer, H. M. Urbassek: Nucl. Instrum. Methods B **73**, 14 (1993) 198
[98] L. Dutkiewicz, R. Pedrys, J. Schou, K. Kremer: Phys. Rev. Lett. **75**, 1407 (1995) 199
[99] J. Schou: Nucl. Instrum. Methods B **27**, 188 (1987) 199
[100] H. M. Urbassek, J. Michl: Nucl. Instrum. Methods B **22**, 480 (1987) 199
[101] D. E. David, J. Michl: Prog. Solid St. Chem. **19**, 283 (1989) 199
[102] D. Fenyö, B. U. R. Sundqvist, B. R. Karlsson, R. E. Johnson: Phys. Rev. B **42**, 1895 (1990) 201, 217
[103] D. Fenyö, R. E. Johnson: Phys. Rev. B **46**, 5090 (1992) 201
[104] H. M. Urbassek, H. Kafemann, R. E. Johnson: Phys. Rev. B **49**, 786 (1994) 201
[105] E. M. Bringa, R. E. Johnson: Nucl. Instrum. Methods B **143**, 513 (1998) 201
[106] E. M. Bringa, R. E. Johnson, L. Dutkiewicz: Nucl. Instrum. Methods B **152**, 267 (1999) 201, 216
[107] E. M. Bringa, R. E. Johnson, M. Jakas: Phys. Rev. B **60**, 15107 (1999) 201
[108] E. M. Bringa, M. Jakas, R. E. Johnson: Nucl. Instrum. Methods B **164-165**, 762 (2000) 201
[109] E. M. Bringa, R. E. Johnson: Surf. Sci. **451**, 108 (2000) 201, 216
[110] M. M. Jakas, E. M. Bringa: Phys. Rev. B **62**, 824 (2000) 201
[111] M. M. Jakas: Radiat. Eff. Defects Solids **152**, 157 (2000) 201
[112] M. M. Jakas, E. M. Bringa, R. E. Johnson: Phys. Rev. B **65**, 165425 (2002) 201
[113] M. M. Jakas: Nucl. Instrum. Methods B **193**, 727 (2002) 201
[114] M. Beuve, N. Stolterfoht, M. Toulemonde, C. Trautmann, H. M. Urbassek: Phys. Rev. B **68**, 125423 (2003) 201
[115] V. I. Shulga, M. Vicanek, P. Sigmund: Phys. Rev. A **39**, 3360 (1989) 201
[116] V. I. Shulga, P. Sigmund: Nucl. Instrum. Methods B **62**, 23 (1991) 201, 202
[117] R. S. Averback, T. Diaz de la Rubia, H. Hsieh, R. Benedek: Nucl. Instrum. Methods B **59/60**, 709 (1991) 201

[118] H. Hsieh, R. S. Averback, H. Sellers, C. P. Flynn: Phys. Rev. B **45**, 4417 (1992) 201
[119] Z. Pan: Nucl. Instrum. Methods B **66**, 325 (1992) 201
[120] R. S. Averback, M. Ghaly: Nucl. Instrum. Methods B **90**, 191 (1994) 201
[121] R. S. Averback, M. Ghaly, H. Zhu: Radiat. Eff. Defects Solids **130-131**, 211 (1994) 201
[122] Z. Y. Pan, M. Hou: Nucl. Instrum. Methods B **102**, 317 (1995) 201
[123] H. Haberland, Z. Insepov, M. Moseler: Phys. Rev. B **51**, 11061 (1995) 201
[124] H. Hsieh, R. S. Averback: Phys. Rev. B **42**, 5365 (1990) 201
[125] H. Hsieh, R. S. Averback: Nucl. Instrum. Methods B **59/60**, 203 (1991) 201
[126] H. Haberland, Z. Insepov, M. Moseler: Z. Phys. D **26**, 229 (1993) 201
[127] T. Aoki, J. Matsuo, Z. Insepov, I. Yamada: Nucl. Instrum. Methods B **121**, 49 (1997) 201, 202
[128] Z. Insepov, I. Yamada: Nucl. Instrum. Methods B **121**, 44 (1997) 201, 202
[129] M. Henkel, H. M. Urbassek: Nucl. Instrum. Methods B **145**, 503 (1998) 201
[130] C. F. Sanz-Navarro, R. Smith, D. J. Kenny, S. Pratontep, R. E. Palmer: Phys. Rev. B **65**, 165420 (2002) 201
[131] Z. Insepov, I. Yamada, M. Sosnowski: Mater. Chem. Phys. **54**, 234 (1998) 201, 202, 204
[132] M. Moseler, O. Rattunde, J. Nordiek, H. Haberland: Nucl. Instrum. Methods B **164-165**, 522 (2000) 201, 204, 212
[133] T. Muramoto, N. Hirotami, K. Itabasi, A. Harada, Y. Yamamura: Nucl. Instrum. Methods B **202**, 289 (2003) 201, 204
[134] K. Johannessen: Nucl. Instrum. Methods B **73**, 481 (1993) 202
[135] M. Lindenblatt, R. Heinrich, A. Wucher, B. J. Garrison: J. Chem. Phys. **115**, 8643 (2001) 202
[136] M. Medvedeva, I. Wojciechowski, B. J. Garrison: Surf. Sci. **505**, 349 (2002) 202
[137] M. H. Shapiro, T. A. Tombrello: Nucl. Instrum. Methods B **152**, 221 (1999) 202
[138] M. H. Shapiro, T. A. Tombrello: Surf. Sci. **453**, 143 (2000) 202
[139] M. H. Shapiro, T. A. Tombrello: Nucl. Instrum. Methods B **217**, 253 (2004) 202
[140] Z. Insepov, I. Yamada: Nucl. Instrum. Methods B **99**, 248 (1995) 202
[141] I. Yamada, J. Matsuo, Z. Insepov, D. Takeuchi, M. Akizuki, N. Toyoda: J. Vac. Sci. Technol. A **14**, 781 (1996) 202
[142] Z. Insepov, I. Yamada: Nucl. Instrum. Methods B **153**, 199 (1999) 202
[143] I. Yamada, J. Matsuo, Z. Insepov, T. Aoki, T. Seki, N. Toyoda: Nucl. Instrum. Methods B **164-165**, 944 (2000) 202
[144] G. Betz, W. Husinsky: Nucl. Instrum. Methods B **122**, 311 (1997) 202
[145] T. J. Colla, R. Aderjan, R. Kissel, H. M. Urbassek: Phys. Rev. B **62**, 8487 (2000) 203, 206, 208
[146] T. J. Colla, H. M. Urbassek: Nucl. Instrum. Methods B **164-165**, 687 (2000) 203, 206, 210
[147] E. Salonen, K. Nordlund, J. Keinonen: Nucl. Instrum. Methods B **212**, 286 (2003) 203
[148] Y. Yamaguchi, J. Gspann: Phys. Rev. B **66**, 155408 (2002) 203
[149] R. Smith, K. Beardmore, A. Gras-Marti, R. Kirchner, R. P. Webb: Nucl. Instrum. Methods B **102**, 211 (1995) 203

[150] Z. Postawa, B. Czerwinski, M. Szewczyk, E. J. Smiley, N. Winograd, B. J. Garrison: Anal. Chem. **75**, 4402 (2003) 203
[151] E. E. Z. Zhurkin, S. K. Kolesnikov: Nucl. Instrum. Methods B **193**, 822 (2002) 203
[152] H. M. Urbassek, W. O. Hofer: K. Dan. Vidensk. Selsk. Mat. Fys. Medd. **43**, 97 (1993) 204, 207
[153] F. Karetta, H. M. Urbassek: Appl. Phys. A **55**, 364 (1992) 204, 205
[154] M. H. Shapiro, T. A. Tombrello: Nucl. Instrum. Methods B **84**, 453 (1994) 204
[155] H. Gades, H. M. Urbassek: Nucl. Instrum. Methods B **103**, 131 (1995) 204, 205
[156] G. P. Können, A. Tip, A. E. de Vries: Radiat. Eff. **21**, 269 (1974) 204, 206
[157] G. P. Können, A. Tip, A. E. de Vries: Radiat. Eff. **26**, 23 (1975) 204, 206
[158] I. S. Bitensky, E. S. Parilis, I. A. Wojciechowski: Nucl. Instrum. Methods B **67**, 595 (1992) 204
[159] G. Betz, W. Husinsky: Nucl. Instrum. Methods B **102**, 281 (1995) 205
[160] C. Staudt, R. Heinrich, A. Wucher: Nucl. Instrum. Methods B **164-165**, 677 (2000) 205, 206
[161] C. Staudt, A. Wucher: Phys. Rev. B **66**, 075419 (2002) 205, 206
[162] L. E. Rehn, R. C. Birtcher, S. E. Donnelly, P. M. Baldo, L. Funk: Phys. Rev. Lett. **87**, 207601 (2001) 206
[163] I. S. Bitensky, E. S. Parilis: Nucl. Instrum. Methods B **21**, 26 (1987) 206
[164] H. M. Urbassek: Nucl. Instrum. Methods B **31**, 541 (1988) 206
[165] A. Wucher, B. J. Garrison: J. Chem. Phys. **105**, 5999 (1996) 206
[166] J. W. Hartman, M. H. Shapiro, T. A. Tombrello: Nucl. Instrum. Methods B **124**, 31 (1997) 206
[167] J. W. Hartman, M. H. Shapiro, T. A. Tombrello: Nucl. Instrum. Methods B **132**, 406 (1997) 206
[168] T. J. Colla, H. M. Urbassek, A. Wucher, C. Staudt, R. Heinrich, B. J. Garrison, C. Dandachi, G. Betz: Nucl. Instrum. Methods B **143**, 284 (1998) 206, 207
[169] T. Muramoto, M. Okai, Y. Yamashita, K. Yorizane, Y. Yamamura: Nucl. Instrum. Methods B **180**, 222 (2001) 206
[170] A. Wucher, N. K. Dzhemilev, I. V. Veryovkin, S. V. Verkhoturov: Nucl. Instrum. Methods B **149**, 285 (1999) 207
[171] R. S. Taylor, B. J. Garrison: Chem. Phys. Lett. **230**, 495 (1994) 208
[172] R. S. Taylor, C. L. Brummel, N. Winograd, B. J. Garrison, J. C. Vickerman: Chem. Phys. Lett. **233**, 575 (1995) 208
[173] R. P. Webb, D. E. Harrison, Jr.: Radiat. Eff. Lett. **86**, 15 (1983) 209
[174] D. E. Harrison, Jr., R. P. Webb: Nucl. Instr. Methods **218**, 727 (1983) 209
[175] M. Ghaly, K. Nordlund, R. S. Averback: Philos. Mag. A **79**, 795 (1999) 209
[176] H. Gades, H. M. Urbassek: Phys. Rev. B **50**, 11167 (1994) 209, 210
[177] C. Busse, C. Engin, H. Hansen, U. Linke, T. Michely, H. M. Urbassek: Surf. Sci. **488**, 346 (2001) 209
[178] E. M. Bringa, K. Nordlund, J. Keinonen: Phys. Rev. B **64**, 235426 (2001) 210, 211
[179] R. Aderjan, H. M. Urbassek: Nucl. Instrum. Methods B **164-165**, 697 (2000) 210, 211
[180] K. Nordlund: Phys. World **14**, 22 (2001) 210

[181] J. Gspann: in P. Jena, et al. (Eds.): *Physics and Chemistry of Finite Systems*, vol. II (Kluwer, Dordrecht 1992) p. 1115 210
[182] K. Nordlund, K. O. E. Henriksson, J. Keinonen: Appl. Phys. Lett. **79**, 3624 (2001) 211
[183] K. Nordlund, J. Tarus, J. Keinonen, S. E. Donnelly, R. C. Birtcher: Nucl. Instrum. Methods B **206**, 189 (2003) 211
[184] R. C. Birtcher, S. E. Donnelly: Phys. Rev. Lett. **77**, 4374 (1996) 211
[185] S. E. Donnelly, R. C. Birtcher: Phys. Rev. B **56**, 13599 (1997) 211
[186] E. M. Bringa, R. E. Johnson, R. Papaleo: Phys. Rev. B **65**, 094113 (2002) 211
[187] E. M. Bringa, E. Hall, R. E. Johnson, R. Papaleo: Nucl. Instrum. Methods B **193**, 734 (2002) 211
[188] P. Sigmund: J. Mater. Sci. **8**, 1545 (1973) 212
[189] U. Littmark, W. O. Hofer: J. Mater. Sci. **13**, 2577 (1978) 212
[190] T. J. Colla, H. M. Urbassek: Nucl. Instrum. Methods B **117**, 361 (1996) 212
[191] G. Betz, M. J. Pellin, J. W. Burnett, D. M. Gruen: Nucl. Instrum. Methods B **58**, 429 (1991) 212
[192] V. A. Zinovyev, L. N. Aleksandrov, A. V. Dvurechenskii, K.-H. Heinig, D. Stock: Thin Solid Films **241**, 167 (1994) 212
[193] P. Bedrossian, T. Klitsner: Phys. Rev. B **44**, 13783 (1991) 212
[194] A. M. Mazzone: Nucl. Instrum. Methods B **160**, 38 (2000) 213
[195] A. M. Mazzone: Nucl. Instrum. Methods B **183**, 251 (2001) 213
[196] J. Jacobsen, B. H. Cooper, J. P. Sethna: Phys. Rev. B **58**, 15847 (1998) 213, 215
[197] M. H. Shapiro, T. A. Tombrello: Nucl. Instrum. Methods B **194**, 425 (2002) 213
[198] A. Friedrich, H. M. Urbassek: Surf. Sci. **547**, 315 (2003) 213
[199] H. Hansen, C. Polop, T. Michely, A. Friedrich, H. M. Urbassek: Phys. Rev. Lett. **92**, 246106 (2004) 213
[200] M. A. Karolewski: Nucl. Instrum. Methods B **211**, 190 (2003) 213
[201] J. M. Pomeroy, A. Couture, J. Jacobsen, B. H. Cooper, J. P. Sethna, J. D. Brock: Mater. Res. Soc. Symp. Proc. **672**, O2.9.1 (2001) 215
[202] J. M. Pomeroy, A. Couture, J. Jacobsen, C. C. Hill, J. P. Sethna, B. H. Cooper, J. D. Brock: Mater. Res. Soc. Symp. Proc. **648**, P7.3.1 (2001) 215
[203] J. E. Rubio, L. A. Marqués, L. Pelaz, M. Jaraíz, J. Barbolla: Nucl. Instrum. Methods B **112**, 156 (1996) 215
[204] L. A. Marqués, J. E. Rubio, M. Jaraíz, L. A. Bailón, J. Barbolla: J. Appl. Phys. **81**, 1488 (1997) 215
[205] E. F. C. Haddeman, B. Thijsse: Nucl. Instrum. Methods B **202**, 161 (2003) 215
[206] Y. Zhong, Y. Ashkenazy, K. Albe, R. S. Averback: J. Appl. Phys. **94**, 4432 (2003) 215
[207] D. E. Hanson, B. C. Stephens, C. Saravanan, J. D. Kress: J. Vac. Sci. Technol. A **19**, 820 (2001) 215
[208] J. Peltola, K. Nordlund, J. Keinonen: Nucl. Instrum. Methods B **206**, 61 (2003) 215
[209] M. A. Karolewski: Nucl. Instrum. Methods B **225**, 217 (2004) 215
[210] H. Kafemann, H. M. Urbassek: Mod. Phys. Lett. B **7**, 857 (1993) 216

[211] D. W. Brenner, B. J. Garrison: Phys. Rev. B **34**, 5782 (1986) 216
[212] L. Dutkiewicz, R. E. Johnson, A. Vertes, R. Pedrys: J. Phys. Chem. **A 103**, 2925 (1999) 216
[213] S. T. Cui, R. E. Johnson: Int. J. Quantum Chem. **23**, 575 (1989) 217
[214] S. Banerjee, R. E. Johnson: Int. J. Quantum Chem. **41**, 383 (1992) erratum 217
[215] S. Banerjee, R. E. Johnson, S. Cui, P. T. Cummings: Phys. Rev. B **43**, 707 (1991) 217
[216] S. Banerjee, M. Liu, R. E. Johnson: Surf. Sci. Lett. **255**, L504 (1991) 217
[217] B. J. Garrison, A. Delcorte, K. D. Krantzman: Acc. Chem. Res. **33**, 69 (2000) 217
[218] B. J. Garrison: in J. C. Vickerman, D. Briggs (Eds.): *ToF-SIMS: Surface Analysis by Mass Spectrometry* (IM Publications, Chichester 2001) p. 223 217
[219] L. V. Zhigilei, P. B. S. Kodali, B. J. Garrison: J. Phys. Chem. **101**, 2028 (1997) 217
[220] L. V. Zhigilei, B. J. Garrison: J. Appl. Phys. **88**, 1281 (2000) 217
[221] D. W. Brenner: Phys. Rev. B **42**, 9458 (1990) 217, 218
[222] D. W. Brenner: Phys. Rev. B **46**, 1948 (1992) erratum 217, 218
[223] S. J. Stuart, A. B. Tutein, J. A. Harrison: J. Chem. Phys. **112**, 6472 (2000) 217
[224] K. D. Krantzman, Z. Postawa, B. J. Garrison, N. Winograd, S. J. Stuart, J. A. Harrison: Nucl. Instrum. Methods B **180**, 159 (2001) 217
[225] Z. Postawa, K. Ludwig, J. Piaskowy, K. Krantzman, N. Winograd, B. J. Garrison: Nucl. Instrum. Methods B **202**, 168 (2003) 217
[226] A. Delcorte, B. J. Garrison: J. Phys. Chem. B **104**, 6785 (2000) 217
[227] R. Chatterjee, Z. Postawa, N. Winograd, B. J. Garrison: J. Phys. Chem. B **103**, 151 (1999) 217
[228] K. Beardmore, R. Smith: Nucl. Instrum. Methods B **102**, 223 (1995) 218
[229] A. Delcorte, P. Bertrand, B. J. Garrison: J. Phys. Chem. B **105**, 9474 (2001) 218
[230] B. J. Garrison, D. Srivastava: Ann. Rev. Phys. Chem. **46**, 373 (1995) 218
[231] D. W. Brenner: MRS Bull. **21**, 36 (1996) 218
[232] E. Salonen, K. Nordlund, J. Keinonen, C. H. Wu: Europhys. Lett. **52**, 504 (2000) 218
[233] K. Nordlund, E. Salonen, J. Keinonen, C. H. Wu: Nucl. Instrum. Methods B **180**, 77 (2001) 218
[234] E. Salonen, K. Nordlund, J. Keinonen, C. H. Wu: Phys. Rev. B **63**, 195415 (2001) 218
[235] T. A. Schoolcraft, B. J. Garrison: J. Am. Chem. Soc. **113**, 8221 (1991) 218
[236] H. Feil, J. Dieleman, B. J. Garrison: J. Appl. Phys. **74**, 1303 (1993) 218
[237] H. Feil: Phys. Rev. Lett. **74**, 1879 (1995) 218
[238] P. C. Weakliem, C. J. Wu, W. A. Carter: Phys. Rev. Lett. **69**, 200 (1992) 218
[239] M. V. R. Murty, H. A. Atwater: Phys. Rev. B **51**, 4889 (1995) 218
[240] M. E. Barone, D. B. Graves: J. Appl. Phys. **78**, 6604 (1995) 218
[241] M. E. Barone, D. B. Graves: Plasma Sources Sci. Technol. **5**, 187 (1996) 218
[242] M. E. Barone, D. B. Graves: J. Appl. Phys. **77**, 1263 (1995) 218
[243] F. H. Stillinger, T. A. Weber: Phys. Rev. B **31**, 5262 (1985) 218
[244] C. F. Abrams, D. B. Graves: J. Appl. Phys. **86**, 5938 (1999) 219

[245] S. Chiba, T. Aoki, J. Matsuo: Nucl. Instrum. Methods B **180**, 317 (2001) 219
[246] T. Aoki, J. Matsuo, I. Yamada: Nucl. Instrum. Methods B **180**, 164 (2001) 219

Index